Marine and Petroleum Geology 120 (2020) 104567

Contents lists available at ScienceDirect

Marine and Petroleum Geology

journal homepage: www.elsevier.com/locate/marpetgeo

Research paper

Origin and implications of early diagenetic quartz in the Mississippian Bowland Shale formation, Craven Basin, UK

Joseph F. Emmings [a,b,*], Patrick J. Dowey [c], Kevin G. Taylor [c], Sarah J. Davies [b], Christopher H. Vane [a], Vicky Moss-Hayes [a], Jeremy C. Rushton [a]

[a] British Geological Survey, Keyworth, Nottingham, NG12 5GG, UK
[b] School of Geography, Geology and the Environment, University of Leicester, Leicester, LE1 7RH, UK
[c] Department of Earth and Environmental Sciences, The University of Manchester, Oxford Road, Manchester, M13 9PL, UK

ARTICLE INFO

Keywords:
Mudstone
Diagenesis
Quartz
Cement
Porosity
Compaction

ABSTRACT

Silica cementation exerts a key control on the compaction and geotechnical properties of mudstones, and by extension, the style of hydrocarbon and/or mineral systems present in a given sedimentary basin. Integrated microscopic and bulk geochemical observations demonstrate that siliceous mudstones in the Bowland Shale Formation, a target for UK shale gas extraction, exhibit abundant dispersed, discrete, μm-scale quartz cements, and exhibit silica enrichment ('excess') above a local detrital Si/Al threshold of 2.5. Dissolution of siliceous radiolarian tests during early diagenesis is identified as the main source of silica (opal A) required for quartz precipitation, either via opal CT or directly to quartz, and potentially generated as a product of anoxic marine 'weathering' (dissolution) of reactive silicates during early diagenesis. Excess silica correlates with free hydrocarbons (S1) normalised to total organic carbon (oil saturation index; OSI); we propose early diagenetic quartz precipitation suppressed pore collapse ('buttress effect'), retaining the pore space capacity to host oil. Quartz precipitation was likely catalysed, for example via low porewater pH, elevated Al and/or Fe oxide content, and/or abundant labile organic matter. Juxtaposition of siliceous mudstones and mudstones lacking quartz cement indicates silica was immobile beyond the bed scale. Thus metre-scale siliceous packages likely represent more prospective units within the Bowland Shale (in terms of unconventional hydrocarbons), on the basis of early diagenetic biogenic-derived quartz cementation leading to improved hydrocarbon storage capacity coupled to enhanced brittleness. These findings are relevant for shale oil and shale gas systems, specifically where oil retained in pores subsequently cracks to generate gas. These findings also suggest the Bowland Shale is a subclass of black shale, defined by the potential to host a relatively large volume of early diagenetic fluids, derived from anoxic bottom waters, which were potentially S- and/or metal-bearing. This is potentially relevant for understanding the genesis of adjacent and related Pb-Zn mineral deposits.

1. Introduction

Silica cementation exerts a key control on the compaction (e.g., White et al., 2011) and geotechnical properties (e.g., Peng et al., 2020) of mudstones, critical for understanding unconventional hydrocarbon source rock prospectivity (e.g., brittleness; Slatt, 2011; Rybacki et al., 2016). Quartz cementation can inhibit mudstone compaction (e.g., Fishman et al., 2015; Milliken and Olson, 2017) which, by extension, suggests it may control the timing of fluid expulsion; with relevance to understanding conventional hydrocarbon systems, and mineral systems linked to mudstone diagenesis (e.g., Frazer et al., 2014). A variety of reactions are attributed to diagenetic quartz genesis in ancient mudstones, which are often temperature, pressure and/or pH-dependent, and catalysed or inhibited by presence of phases such as Fe oxides, clay minerals and Mg hydroxides (e.g., Iler, 1955; Hurd, 1973; Williams and Crerar, 1985; Kastner et al., 1977; Isaacs, 1982; Hinman, 1990; Meister et al., 2014). As a result of this complexity, diagenetic quartz is manifested in mudstones in a range of styles, ranging from quartz-replaced bioclasts (e.g., Kidder and Erwin, 2001), bedded or nodular chert (e.g., Moore, 2008), vein quartz (e.g., Wang et al., 2012) and discrete quartz crystals dispersed within the sedimentary matrix (e.g., Milliken et al., 2016). The consumption of dissolved silica via

* Corresponding author. British Geological Survey, Keyworth, Nottingham, NG12 5GG, UK.
E-mail address: josmin65@bgs.ac.uk (J.F. Emmings).

https://doi.org/10.1016/j.marpetgeo.2020.104567
Received 22 October 2019; Received in revised form 22 June 2020; Accepted 29 June 2020
Available online 4 July 2020

precipitation of authigenic clay minerals (rather than quartz), during early diagenesis of organic and metal-rich sediments, is also a first-order sink for several elements dissolved in seawater, such as K, Mg, Li and F, in addition to Si (see Michalopoulos and Aller, 2004).

Emmings et al. (2020a) demonstrated siliceous (quartz-rich) mudstones are widespread in parts of the Bowland Shale Formation in the Craven Basin (Lancashire, UK). The Bowland Shale is of interest because it is a candidate for unconventional hydrocarbon exploration in the UK and in equivalents across Europe (e.g., Zijp et al., 2017; Whitelaw et al., 2019). The Bowland Shale is also partly age equivalent to the Barnett Shale, USA, a producing unconventional hydrocarbon reservoir (Smith et al., 2011). In addition, the Bowland Shale is a candidate source of metals and/or reduced sulphur (S; e.g., H_2S, polysulphides) which were fed into the adjacent blocks and highs as part of the Pennine lead-zinc (Pb-Zn) mineral system (e.g., Dunham and Wilson, 1985; Kendrick et al., 2002).

Quartz cement is limited to facies linked to deposition under productive water column and anoxic bottom water conditions (Emmings et al., 2019, 2020b). Therefore, by integration of microscopic observations and geochemical data, we explore the nature, origin and importance of quartz in the Bowland Shale. We propose precipitation of discrete, μm-scale quartz crystals, linked to a biogenic source (radiolarian opal A precursor), formed a supporting network ('buttress') within the sedimentary matrix of most anoxic facies in the Bowland Shale. The buttressing effect by early diagenetic quartz suppressed compaction, therefore retaining high fluid storage capacity, in this unit. This is important for understanding the distribution of *in-situ* free hydrocarbons in the Bowland Shale, and suggests the Bowland Shale defines a black shale sub-class defined by the ability to host a relatively large volume of early diagenetic fluids derived from anoxic bottom waters, which were potentially S- and/or metal-bearing.

2. Geological Setting

The Bowland Shale Formation was deposited in a series of fault-bound graben and half-graben structures (Anderson and Underhill, 2020; Fraser and Gawthorpe, 1990), referred to as a 'block and basin' topography (see Emmings et al., 2020a and references therein), in the Rheic-Tethys epicontinental seaway that spanned from present-day North America to Poland. Transition from active rifting to thermal subsidence broadly aligns with subdivision of the Bowland Shale Formation into lower and upper units at the Visean-Serpukhovian boundary (Waters et al., 2009, Fig. 1a). The upper unit of the Mississippian Bowland Shale Formation (Upper Bowland Shale; herein termed 'Bowland Shale'; this study) defines a key transition between the carbonate-dominated Lower Bowland Shale (Newport et al., 2018) and the Millstone Grit Group, a siliciclastic toe-of-slope fan system (Waters et al., 2009).

The switch from rift to thermal sag produced an interdigitating succession of hemipelagic and siliciclastic facies in the Craven Basin (Emmings et al., 2020a; Waters et al., 2019). Sedimentary facies include hemipelagites, turbidites, hybrid event beds and lenticular (mud intraclast-bearing) mudstones (Emmings et al., 2020a). Siliciclastic sediments were supplied primarily from the advancing from the north to north-east (Pendleton Formation; Waters et al., 2009), across and around the Askrigg Block in the north-east (Fig. 1b). Basin water depth likely ranged from ca. 100–200 m (Davies, 2008; Holdsworth and Collinson, 1988). The Bowland Shale was deposited under weakly restricted, dominantly anoxic and intermittently sulphidic bottom water conditions likely driven by primary productivity (Emmings et al., 2019, 2020b).

Deposition was moderated by fourth-order eustatic sea level fluctuations in response to interglacial-glacial cycles on Gondwana (see Waters and Condon, 2012 and references therein). Packages deposited during marine transgressions and/or highstands are termed 'marine bands' and are associated with a macrofaunal body fossil assemblage, used to define biozones including $E_{1a}1$ to $E_{1c}1$ (e.g., Waters and Condon, 2012, Fig. 1a). The inherited carbonate-to-mixed syn-rift system was gradually inundated by siliciclastic submarine turbidite systems as part of the Millstone Grit Group (e.g., Waters et al., 2009, Fig. 1b).

Several phases of intrusive and explosive volcanism occurred during the Mississippian in the UK, although there is no evidence for direct volcanic input (e.g., volcanic glass) into the Craven Basin during deposition of the Bowland Shale. During the Visean and early Namurian, the Midland Valley of Scotland towards the north experienced long-lived volcanism (Browne et al., 1999). Brigantian basaltic lavas, sills and pyroclastic rocks are also present on the Derbyshire Platform and in the adjacent Widmerpool Gulf basin to the south (Ramsbottom et al., 1962; Walters and Ineson, 1981). Several thin Arnsbergian bentonite horizons are also recognised in the Central Pennine Basin (Spears et al., 1999), in similar geographic position to the Craven Basin (Waters et al., 2007).

The hinterland drainage area, feeding rivers linked to the Pendle delta (e.g., Emmings et al., 2020a, Fig. 1b), was probably very large and thus drained a variety of igneous, volcanic and metamorphic rocks (Collinson, 1988; Drewery et al., 1987; Spears, 2006). An anomalously high Se content in the Bowland Shale, compared to other black shales, supports the presence of volcanic rocks in the hinterland (Parnell et al., 2016). Palaeoclimate indicators suggest prevalence of tropical to sub-tropical conditions (Boucot et al., 2013). Lowlands were likely vegetated; the Strait of Malacca in south-east Asia is a candidate modern analogue (Stephenson et al., 2008). Therefore the particulate and dissolved fraction of local rivers, feeding the Pendle delta system, likely included a significant component of physical and chemical weathering products. Dunham and Wilson (1985) and Fairbairn (2001) interpreted time-equivalent chert beds on the Askrigg Block (Fig. 1b) as primary or diagenetic precipitates related to a locally high dissolved silica riverine input, or from hydrothermal vents at seabed (although there is no direct evidence for the latter). Regionally, detrital kaolinite and mixed-layer illite-smectite typically dominate the allochthonous mud fraction (Spears, 2006). The silt to sand-sized fraction typically comprises detrital quartz, feldspar, muscovite, chlorite and heavy minerals such as rutile and magnetite (e.g., Spears, 2006; Brandon et al., 1998; Emmings et al., 2020a; Emmings et al., 2020b).

Variscan inversion of the Craven Basin during the Pennsylvanian generated a set of north-east to south-west trending folds, thrust-folds and monoclines, collectively defined as the Ribblesdale Fold Belt (Arthurton, 1984; Gawthorpe, 1987a; Pharaoh et al., 2019). Maximum burial was likely attained during the Late Cretaceous (Andrews, 2013; Clarke et al., 2018; Pearson and Russell, 2000). An immature to early oil window thermal maturity is expected on the basis of apatite fission-track analysis (Lewis et al., 1992) and illite crystallinity (Waters et al., 2019) measurements for the Bowland Shale at outcrop, textural and isotopic analysis of burial dolomites in the Lower Bowland Shale in the Ribblesdale Fold Belt (Gawthorpe, 1987b) and burial modelling (Pearson and Russell, 2000). Pb-Zn mineralisation on adjacent shelves, including the Askrigg Block, include a suite of deposit sub-classes (e.g., Wilkinson, 2014), which developed primarily along fracture systems (Dunham and Wilson, 1985) during the early Variscan inversion of basin-bound faults (Frazer et al., 2014; Late Westphalian to Stephanian inversion; ca. 304 Ma; e.g., Pharaoh et al., 2019), and potentially continued to the end of the Triassic (e.g., Bouch et al., 2006).

3. Materials and Methods

Sedimentological observations and geochemical data are integrated through the Bowland Shale from a ca. 124 m thick outcrop at Hind Clough, Lancashire, north-west England (British National Grid 364430 453210; 53.973725° lat., −2.543778° long., WGS, 1984) and two nearby ca. 20 m and 67 m thick borehole core sections from the Craven Basin (MHD4 [BGS ID 18006] 367426 446752; 53.915882° −2.497411°; Cominco S9 [BGS ID 32766] 386010 463500; 54.067245° −2.215257°; Fig. 1c), respectively. These open-access datasets are reported by

Emmings et al. (2020a), Emmings et al. (2019) and Emmings (2018).

Sampling was conducted systematically through the outcrop, targeting unweathered material within a stream section (see Emmings et al., 2017), and through each borehole section. Samples were finely powdered prior to bulk geochemical analysis. All geochemical data are reported in Emmings et al. (2020b). Major and trace element concentrations were measured on fused beads (109 samples) and powder briquettes (108 samples) with a PANalytical Axios Advanced X-Ray Fluorescence (XRF) spectrometer using default PANalytical SuperQ conditions. Accuracy and precision are both typically ± 1–2% for Si, Al, Ti and Zr reported in this study. 'Excess silica' was defined by Emmings et al. (2020a) as $Si_{excess} = Si_{total}–2.5(Al)$ *sensu*. Sholkovitz and Price (1980), for example, where 2.5 is a local detrital Si/Al threshold which delineates silica-rich facies. Si/Al = 2.5 does not represent a line of best fit (see Results and Discussion).

110 samples were pyrolised in a Rock-Eval 6™ apparatus (Vinci Technologies), in standard mode, at the British Geological Survey. Accuracy is typically 1–2% for most Rock-Eval parameters, based on repeat analyses of the IFP Rock-Eval standard. Repeat measurements provide estimates for precision (two standard deviations) of ±0.11 mgHC/g and 0.44 mgHC/g, for S1 and S2 parameters, respectively. Total organic carbon (TOC) and inorganic carbon (MINC) precision is estimated at ± 0.03 wt %. Oil saturation index (OSI) is defined as OSI = (S1*100)/TOC. Hydrogen index (HI) is defined as HI = (S2*100)/TOC.

Most samples exhibit RockEval pyrolysis T_{max} between 417 °C and 446 °C (including a bitumen-extracted subset), indicating these samples are thermally immature to early oil mature (Emmings et al., 2019, 2020b). Samples at Cominco S9 exhibit higher T_{max} (437°C–458 °C); this

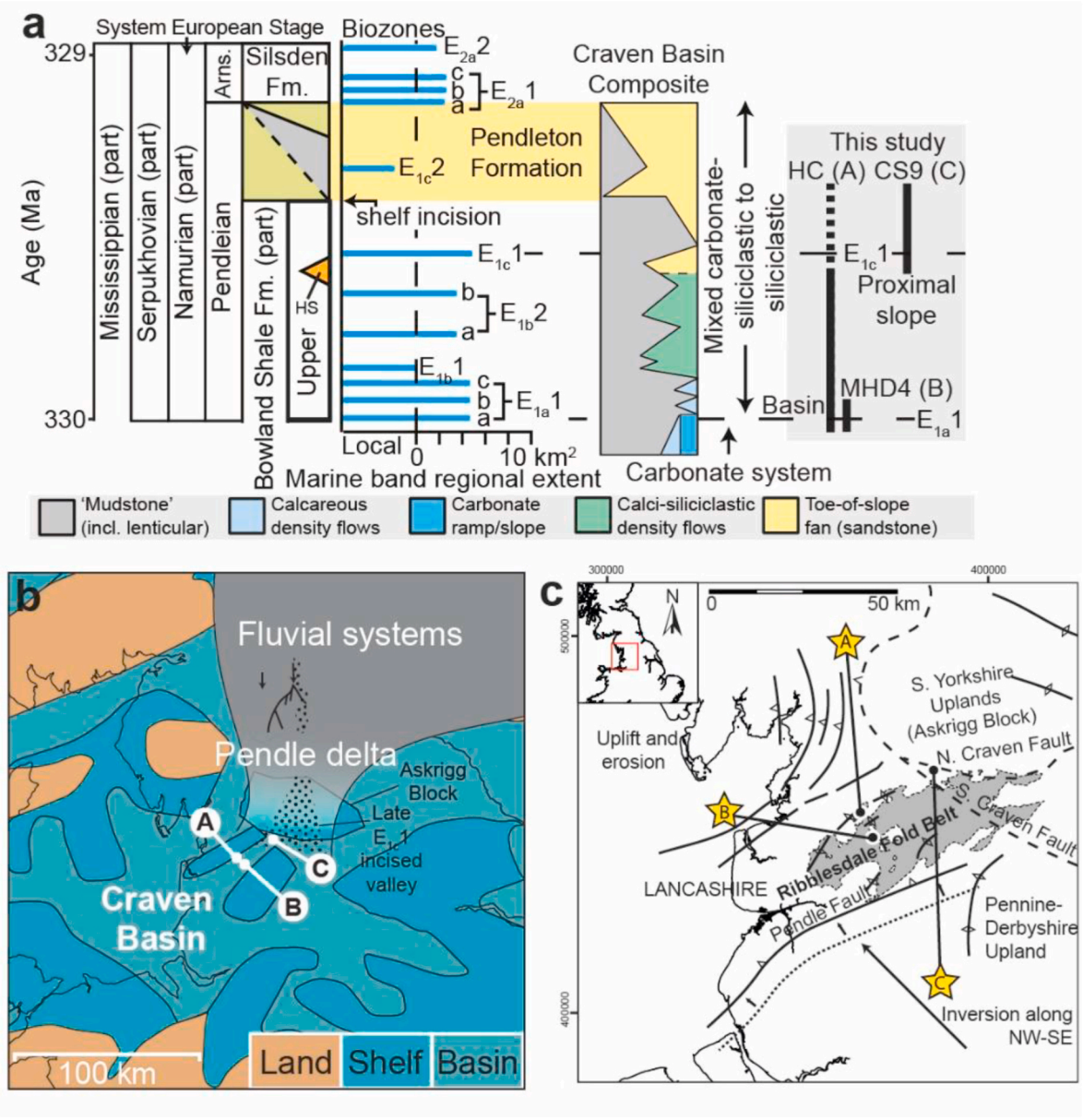

Fig. 1. Stratigraphy and location map for sections. (a) Stratigraphy of the Upper Bowland Shale and Craven Basin composite log modified from Emmings et al. (2019, 2020a) and references therein. Absolute ages and 'marine band' regional extents from Waters and Condon (2012). Arns. = Arnsbergian. HS = Hind Sandstone Member. HC = Hind Clough (Site A; outcrop; see Fig. 2). MHD4 = Marl Hill 4 (Site B; borehole). CS9 = Cominco S9 (Site C; borehole). (b) Inherited Visean regional basin structure, and Pendle delta and feeder system extent, redrawn from Emmings et al. (2020b). Based on observations and interpretations in Bijkerk (2014); Fraser and Gawthorpe (2003); Fraser and Gawthorpe (1990); Waters et al. (2007) and Waters et al. (2014). (c) Location map of the Ribblesdale Fold Belt (Lancashire, UK) including Westphalian-Stephanian structural elements (Fraser and Gawthorpe, 1990) and outcrop extent (DiGMapGB-625, published with permission of the British Geological Survey), redrawn from Emmings et al. (2019). Contains Ordnance Survey data © Crown Copyright and database rights. Study sites as labelled in (a).

potentially indicates higher thermal maturity (i.e., late oil window) or may relate to matrix effects (Emmings et al., 2020b). Thermal maturity was also estimated using Laser Raman spectroscopic analysis of phytoclasts, using two samples from Hind Clough (samples 04B and 73; Henry et al., 2018). The lowest G-band full-width half-maximum and scaled spectrum area parameters were selected for each sample (2σ of mean values as reported in Henry et al., 2018). Vitrinite reflectance was estimated ($_{eq}VR_o$) using calibration curves of Henry et al. (2019). $_{eq}VR_o$ between 0.7 and 1.3% suggests burial into the early to late oil window for samples at Hind Clough (e.g., Merriman and Kemp, 1996). Burial to the base of the early oil window (ca. 90–110 °C) is consistent with regional estimates for maximum burial (see Geological Setting).

A subset of 37 samples, spanning the observed sedimentary and geochemical heterogeneity, were cut into 'ultrathin' 20 μm thick, polished and uncovered thin sections and studied under optical and reflected light using a standard petrological microscope. Scanning electron microscopy (SEM) was conducted using an S-3600N Hitachi microscope with Oxford INCA 350 EDS at the University of Leicester, and a JEOL JXA-8530F Hyperprobe microscope equipped with a JEOL panchromatic cathodoluminescence (SEM-CL) detector at the University of Manchester. False colour composite SEM–EDS images were compiled using Fiji (ImageJ) software and overlain onto each corresponding BSE microphotograph. Elements were mapped to red (R), green (G) or blue (B) channels (as annotated on the respective figure).

4. Results and Discussion

Of the ten sedimentary facies (A-J) defined in Fig. 2 (see also Emmings et al., 2019, 2020a), Facies A-F samples exhibit 'excess silica' (i.e., Si/Al > 2.5; see discussion below; Figs. 2–3a; Emmings et al., 2020a). Al is utilized as a proxy for the detrital clay fraction (e.g., Hild and Brumsack, 1998), where detrital clays plot with Si/Al < 2.5 (Fig. 3a). Claystone and siltstone facies (H-I), present only in Cominco S9 proximal to the Pendle delta (Fig. 1), typically also exhibit Si/Al < 2.5. Petrographic observations and qualitative XRD data (Emmings et al., 2020a) indicate feldspar content is relatively low, suggesting Al content is dominantly a proxy for clay minerals (rather than feldspars). The coefficient of variation of Al is 0.52, similar to trace elements (mean coefficient of variation = 0.66), supporting Al-normalization (see Tribovillard et al., 2006). Si/Al > 2.5 is observed in all Facies A-F samples

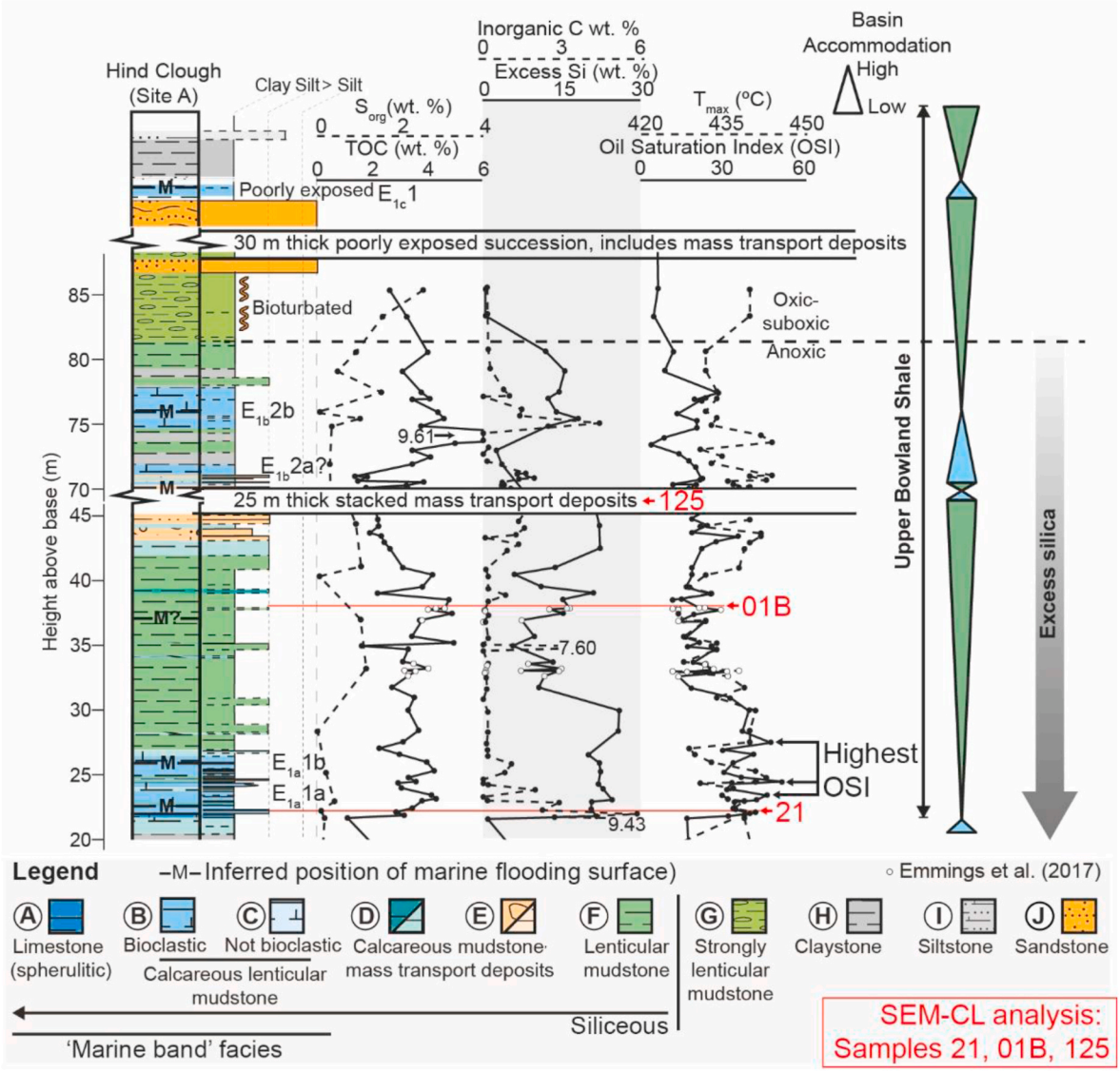

Fig. 2. Sedimentary log through Hind Clough outcrop after Emmings et al. (2019, 2020a), including positions of key thin section SEM analyses (this study). Palynological data, geochemical data and interpretations compiled from Emmings et al. (2019, 2020a, 2020b). S_{org} = organic S (methodology in Emmings et al., 2020b).

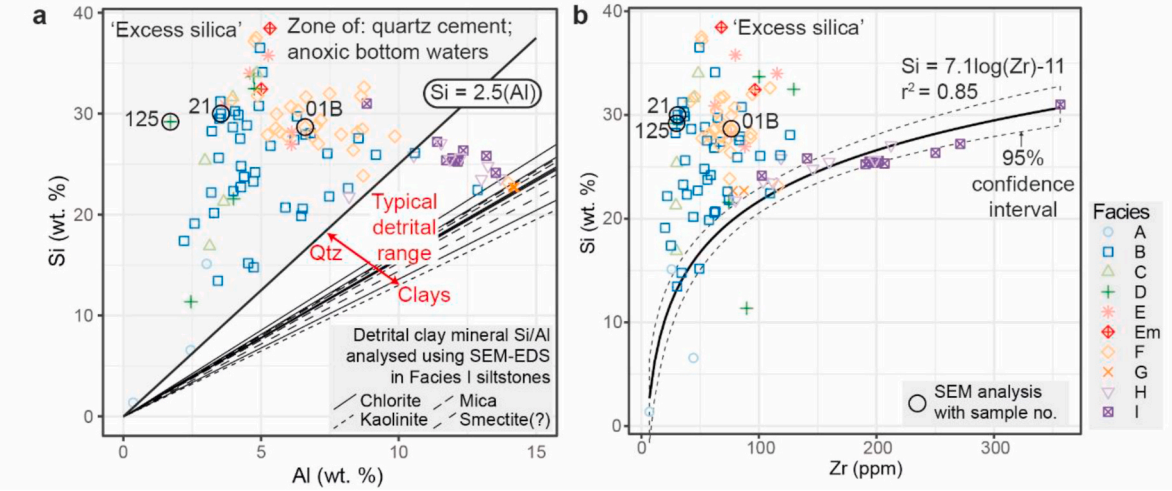

Fig. 3. XRF analyses plotted for all sedimentary facies. (a) Si versus Al plot shows all siliceous mudstones (Facies A-F) contain 'excess silica' above a local basin threshold of Si = 2.5Al, as defined by Emmings et al. (2020a). Detrital clay mineral Si/Al ratios in Facies I determined using SEM-EDS are also plotted. Si/Al variation within Facies G-I, below Si/Al = 2.5, indicates variable proportions of detrital quartz silt (labelled Qtz) and detrital clays. Samples which exhibit Si/Al > 2.5 contain quartz cements (with the exception of one Facies I sample; see discussion). Palaeoredox proxies indicates the zone above Si/Al = 2.5 also delineates deposition under anoxic bottom water conditions (Emmings et al., 2020b) (b) Si versus Zr plot supports the definition of 'excess silica', where most Facies A-F data plot above Si = 7.1log(Zr)–11 (analogous to the detrital fit of Dowey and Taylor, 2019 for the Haynesville-Bossier Shale). Facies G samples plot with marginal Si/Zr enrichment, and contain nodules of stacked kaolinite booklets but lack quartz cement (Emmings et al., 2020a). This suggests localised, fully coupled Si and Al mobility during diagenesis of Facies G.

to below the contact with Facies G at approximately 81 m above base, at the outcrop Hind Clough (Fig. 2).

The high Si/Al in Facies A-F is best explained by abundant: (i) detrital quartz silt (where input was decoupled from the detrital Al supply); and/or (ii) preserved biogenic skeletal material; and/or (iii) quartz cement. In order to resolve the potential for detrital quartz as an explanation for the high Si/Al ('excess silica'), Zr is utilized as a proxy for the silt to sand-sized detrital fraction (i.e., zircon heavy minerals expected to partition with detrital quartz; e.g., Hild and Brumsack, 1998; Wright et al., 2010; Davies et al., 2012; Dowey and Taylor, 2017, Dowey and Taylor, 2019). Zr content is highest in Facies H-I (Fig. 3b), consistent with petrographic observations which shows abundant silt to sand-sized detrital grains in these proximal mudstones and siltstones (such as quartz, chlorite, feldspar, heavy minerals; see Emmings et al., 2020a). Thus Facies H-I Si/Al variation between Si/Al = 2.5 and detrital clays (Fig. 3a) is best explained by changing proportions of detrital quartz silt and detrital clay minerals.

Unlike Facies H-I, the lack of correlation between Zr and Si for Facies A-F (Fig. 3b) suggests the high Si/Al is not related to detrital quartz silt or sand content. This is supported by BSE and SEM-CL imaging (*sensu*. Schieber et al., 2000), which shows detrital quartz grains are rare in Facies A-F (Fig. 4). In few cases, low luminescence overgrowths are developed on high luminescence detrital grains (Fig. 4i). Siliceous bioclasts (such as radiolarian tests, sponge spicules) are also rare to absent in the matrix of Facies A-F. Instead, SEM-CL shows presence of highly abundant, matrix-dispersed mm to nm-scale quartz cements (Fig. 4), which are absent in Facies H-I (Emmings et al., 2020a). Thus Si/Al > 2.5 delineates the zone where all samples contain quartz cements (Fig. 3a). This zone also delineates deposition under anoxic bottom water conditions (Emmings et al., 2020b). One Facies I siltstone is an exception, because it exhibits Si/Al > 2.5 but lacks silica cement; this shows Si/Al is an imperfect proxy for 'excess silica' and therefore should be supported by textural observations and assessment of Si/Zr, for example (Fig. 3b). In all other cases, increasing detrital quartz silt content is not a credible explanation for the 'excess silica' component defined using Si/Al.

Potential sources of the quartz cements are: (i) the dissolution (and re-precipitation) of nearly completely amorphous biogenic silica (e.g., Lancelot, 1973; Schink et al., 1975), opal A, to more thermodynamically stable (lower entropy) forms; via opal CT to quartz (e.g., Isaacs, 1982; Rice et al., 1995; Milliken et al., 2016; Milliken and Olson, 2017), or directly to quartz (i.e., without an intermediate CT phase; e.g., Keene, 1975; Kastner et al., 1977; Meister et al., 2014); (ii) precipitation of quartz as a product of anoxic marine silicate weathering, where CO_2 reacts with silicate phases to produce cation-depleted silicates, HCO_3^-, cations, and dissolved silica (e.g., Wallmann et al., 2008; *sensu* Mackenzie and Garrels, 1966); (iii) the dissolution of detrital K-feldspar (see Yuan et al., 2019 and references therein) or other reactive detrital silicate phases such as mica (e.g., Boles and Franks, 1979) and volcanic glass (White et al., 2011); (iv) the transformation of smectite to illite (e.g., Perry and Hower, 1972; Merriman and Kemp, 1996; Thyberg et al., 2010), and; (v) other external sources, such as intrusions and/or seabed hydrothermal vents. For example, chert nodules in pelagic sediments in the Pacific derive from the circulation of hydrothermal fluids derived from underlying basaltic crust (e.g., Moore, 2008). Fluids derived from felsic intrusions (i.e., potentially oversaturated with respect to silica) are also often associated with a variety vein and/or bedded quartz textures within overlying sedimentary rocks (e.g., Wang et al., 2012). Where Fe-bearing hydrothermal fluids reach seabed, reaction with relatively silica-rich Palaeozoic seawater likely explains the genesis and distribution of hematitic chert (jasper) deposits in the rock record (Grenne and Slack, 2003).

The juxtaposition of siliceous mudstones (Facies A-F) and mudstones/siltstones lacking silica cementation (Facies G-I; Fig. 2, see also Emmings et al., 2020a), indicates silica was strata-bound and immobile beyond the lamina/bed scale (i.e., cm-scale). Low mobility was likely due to low permeability and diffusion coefficients (Bjørlykke, 2011) and/or presence of catalysts which decreased silica solubility. Factors controlling silica solubility (in addition to temperature and pressure) include biogenic particle specific surface area (e.g., Hurd, 1973), Al availability (e.g., Van Beueskom et al., 1997; Hinman, 1998; Dixit et al., 2001), Fe oxide availability (e.g., Grenne and Slack, 2003; see also Meister et al., 2014 and references therein) typically coupled to redox conditions (Michalopoulos and Aller, 1995; Morris and Fletcher, 1987), Mg hydroxide availability (e.g., Iler, 1955; Kastner et al., 1977), organic matter abundance and type (Hinman, 1990), detrital clay mineral abundance and type (Isaacs, 1982) and porewater pH (e.g., Hurd, 1973;

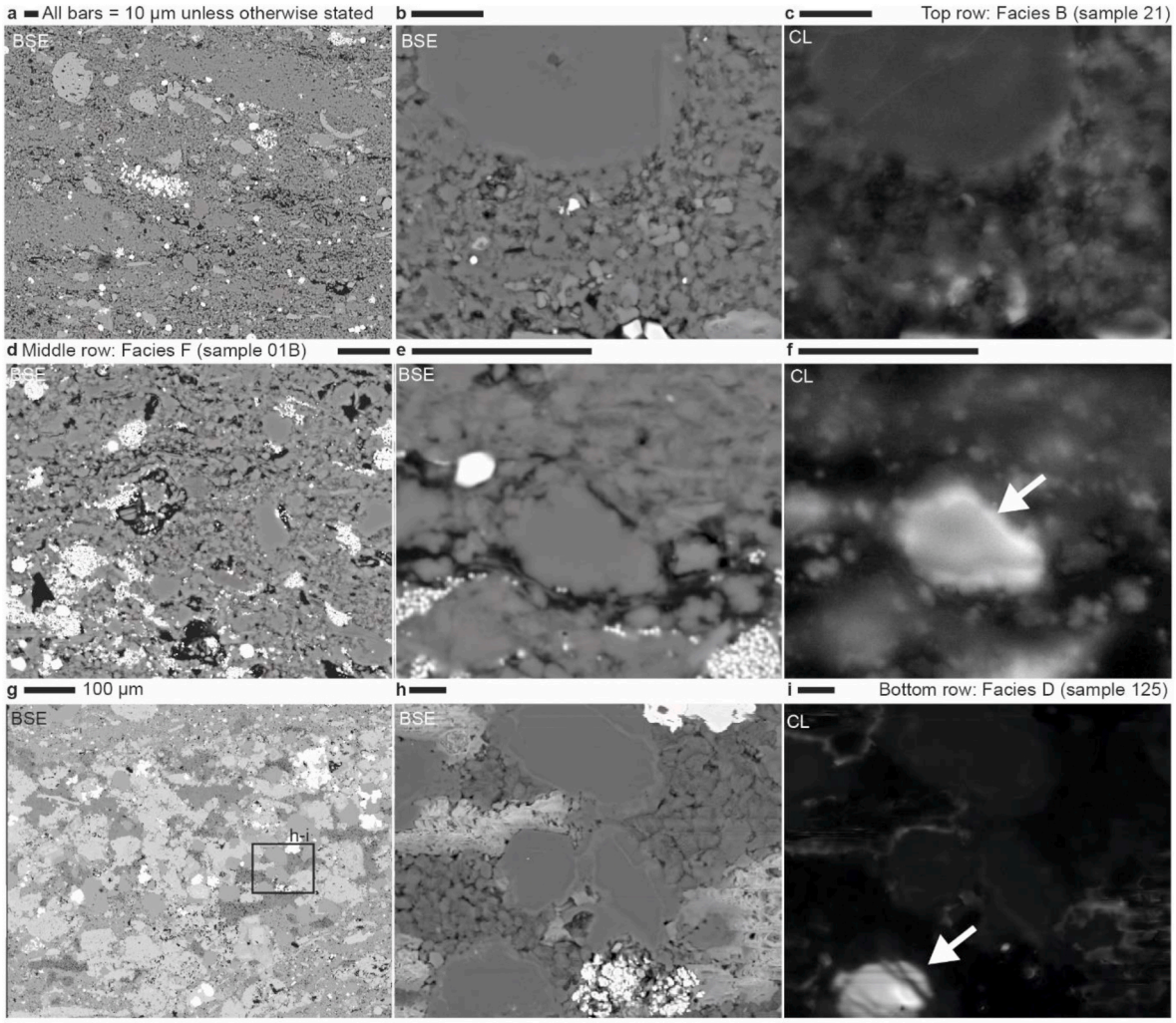

Fig. 4. Scanning electron microphotographs focussed on quartz cements in Facies A-F, imaging backscattered electrons (BSE) and cathodoluminescence (CL), in samples 21, 125 and 04B (see Fig. 2). (a–c) Weakly lenticular bioclastic mudstone (Facies B; 'marine bands') including abundant quartz cements. Low luminescence suggests detrital quartz is absent. (d–f) Lenticular mudstone (Facies F) including rare fine detrital quartz grains, often mantled by nm-scale quartz cements (arrow in f). nm-scale quartz cements are widespread in the matrix of Facies B-F. (g–i) Relatively coarse-grained calciturbidite silt laminae (Facies D), with interlocking quartz-calcite-dolomite-kaolinite-monosulphide cements. Quartz crystals are dominantly diagenetic, which may mantle detrital quartz grains (arrow in i). Stacked book-like kaolinite cement suggests coupled, relatively early diagenetic Si and Al mobility.

Williams and Crerar, 1985). Low porewater pH, elevated Al and/or Fe oxide content, high alkalinity, and/or abundant labile organic matter, as catalysers of quartz precipitation, are all plausible given the depositional setting (i.e., an anoxic, carbonate-, metal- and organic-rich setting, with a high mean sediment accumulation rate, proximal to riverine input; Emmings et al., 2020a; Emmings et al., 2020b). Clay minerals and organic matter are thought to retard opal CT precipitation whereas elevated alkalinity (i.e., associated with dissolved carbonate) promotes opal CT nucleation and may accelerate quartz precipitation (e.g., Kastner et al., 1977; Isaacs, 1982).

The Si/Al ratio of Facies A-F exceeds the stoichiometric composition of feldspar and dioctahedral (i.e., Al-rich) smectite, indicating closed-system feldspar dissolution or smectite to illite transformation are unlikely mechanisms for generation of quartz-cements. Furthermore, smectite to illite transformation is a relatively late diagenetic reaction (between ca. 60–100 °C; e.g., Thyberg et al., 2010); this is contrary to the evidence for early silica mobility in most anoxic facies (Fig. 4a–c; 5a-d). Quartz cement infills pores within organic matter (Fig. 5a; see also Emmings et al., 2020a) and potentially infills bioclast-sheltered pores in Facies B (Fig. 5c and d), suggesting an early diagenetic origin (e.g., Taylor and Macquaker, 2014). The most common quartz cement style is defined by discrete equant crystals dispersed throughout the matrix of Facies B-C and E-F, including infill of pores within organic matter (e.g., Fig. 5a; see also Emmings et al., 2020a). This texture differs from the sheet-like, amalgamated quartz cements that are likely associated with smectite-illite transformation (Thyberg and Jahren, 2011). Kaolinite cement (with apparently randomly oriented booklets) in silty laminae (Facies D; Fig. 4h), and presence of nodules of randomly oriented kaolinite booklets in Facies F and G (Emmings et al., 2020a), also suggests early diagenetic mobility of Si and Al. The relatively high abundance of quartz cement in Facies B-C and F (at least ca. 50% by volume; e.g., Fig. 5a) suggests precipitation within 10s–100 s m of seabed, assuming a mud-rich compaction curve (Kominz et al., 2011; Velde, 1996) and that the quartz cement filled open pores (e.g., Milliken et al., 2016; Milliken and Olson, 2017).

Facies D, and Facies E basal beds (Fig. 3; herein included as part of Facies D), are grain size-fractionated deposits interpreted to represent grain deposition from turbulent and hybrid flows, respectively (i.e., as silic-calci-turbidites and hybrid beds; see Emmings et al., 2020a). Thus a biogenic or siliciclastic 'silt' or 'sand'-rich compaction curve (e.g., Kominz et al., 2011), defined by subdued closure of primary porosity, may best describe the compaction of Facies D. On this basis, quartz

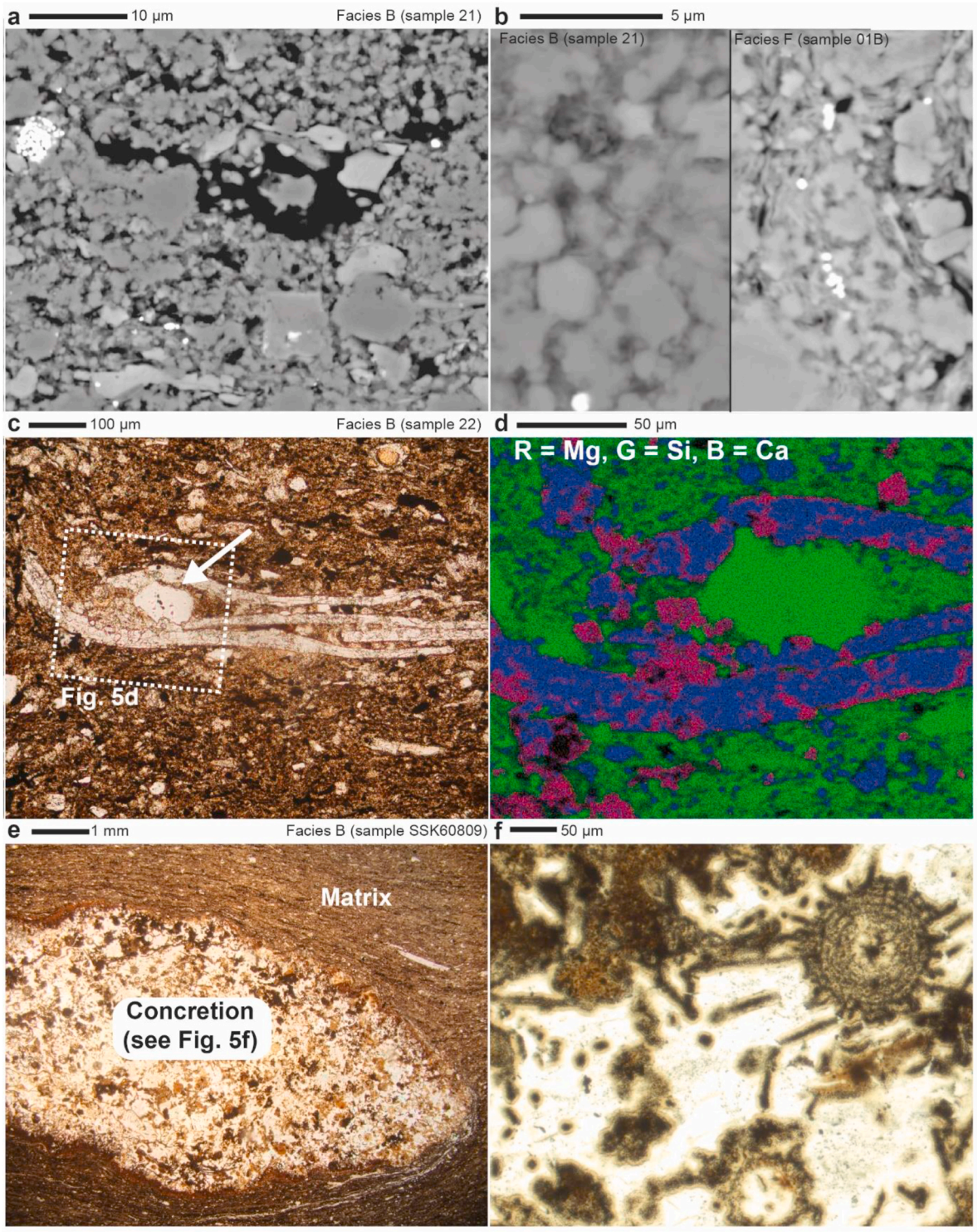

Fig. 5. Example transmitted light and scanning electron microphotographs.(a–b) Additional examples of the nm to μm-scale quartz cements present in Facies B-C and E-F. Note the matrix of sample 21 (a; b, left panel) also contains dispersed calcite cements. (c–d) Typical weakly 'lenticular' and bioclastic mudstone texture of Facies B, including quartz hosted within a skeletal (trilobite) cavity (white arrow). This texture may represent authigenic quartz cement within the shelter porosity of a trilobite test, requiring precipitation during very early diagenesis and under relatively acidic (but potentially high alkalinity) conditions. In the absence of CL imaging for this sample, however, an alternative interpretation favours pressure solution along the contacts between skeletal calcite and a fractured detrital quartz grain. Note also partial replacement of the primary calcite by dolomite (high-Mg areas of bioclast). (e) Early diagenetic calcite-phosphate concretion containing abundant radiolarian tests, such as spumellarian entactinids (Casey, 1993). (f). Detail of abundant radiolarian tests within the concretions, where tests are typically absent in the adjacent matrix. (c,e) are reproduced from Emmings et al. (2020a).

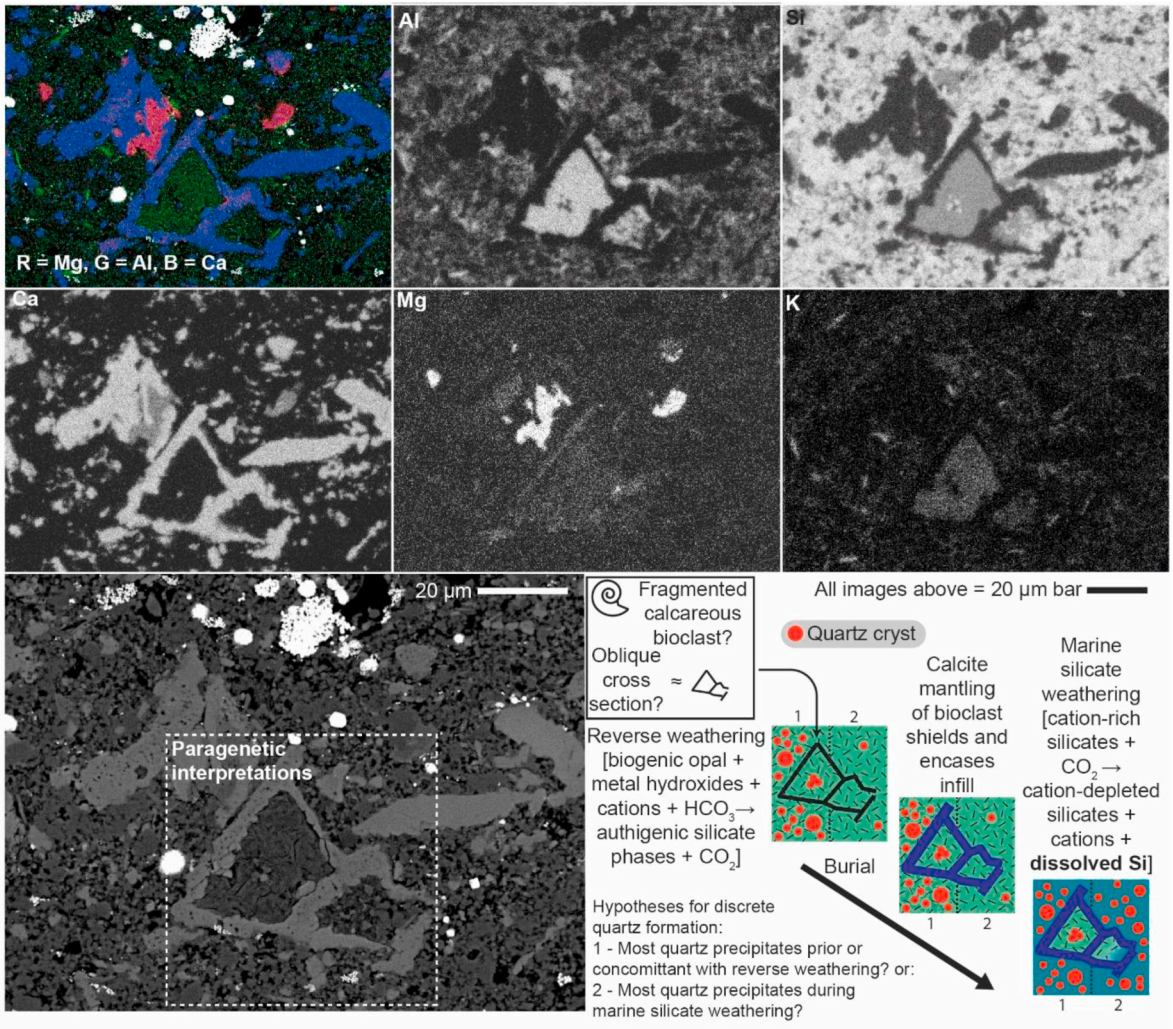

Fig. 6. SEM-EDS imaging as evidence for early diagenetic silicate precipitation (sample 21). Reverse and marine weathering reactions from Wallmann et al. (2008). RGB composite from Emmings et al. (2020a).

cementation in Facies D likely proceeded within ca. 1000 m of seabed (Kominz et al., 2011), therefore also during early diagenesis but potentially later than quartz cementation in Facies B-C and E-F.

The evidence for early diagenetic quartz precipitation implies dissolution of detrital K-feldspar and mica, as key late diagenetic sources of K required for illitization (Boles and Franks, 1979), is an unlikely candidate for the majority of quartz cement observed. Thus open-system silica input derived from feldspar dissolution or smectite to illite transformation is not supported. The quartz textures observed (e.g., partially pore-filling and discrete, equant crystals disseminated through the sedimentary matrix; Fig. 5a–d) are also not comparable to quartz associated with hydrothermal fluids (e.g., quartz veins, nodular or bedded chert, jasper, etc.). There is also no direct evidence for hydrothermal seabed vents and/or intrusions within the Craven Basin; thus other external sources of silica not supported.

Therefore the best explanation for the source of quartz cements is either dissolution of opal A (biogenic silica) and precipitation as quartz (Eq. (1)), and/or precipitation of quartz as a product of anoxic marine weathering of reactive silicates (Fig. 6; Eq. (2); Wallmann et al., 2008). Evidence (e.g., infill of shelter porosity; Fig. 5c and d) suggests at least some silica precipitated rapidly, thus without an intermediate CT phase. Such silica precipitation reactions are dependent on availability of catalysts (or retardants; see above) and temperature. Quartz precipitation typically proceeds during relatively late diagenetic conditions (for example between 50 °C and 110 °C; Murata and Larson, 1975), although catalysts promote lower temperature precipitation (i.e., during early diagenesis) (Behl, 2011; Behl and Garrison, 1994; Meister et al., 2014). Anoxic marine silicate weathering is equivalent to chemical weathering of silicates exposed on the continents; dissolution of detrital reactive silicates in sediment porewaters is a sink for CO_2 and a source of alkalinity. Operation of silicate weathering is consistent with the evidence for an anoxic, organic-rich setting and shallow methanogenesis (Emmings et al., 2020b).

$$\text{Opal A} \rightarrow \text{Opal CT} \rightarrow \text{Quartz} \quad (1)$$

$$\text{Cation-rich silicates} + CO_2 \rightarrow \text{cation-depleted silicates} + \text{dissolved cations} + \text{dissolved silica} + HCO_3^- \quad (2)$$

Carbonate-and-phosphate cemented concretions, interpreted as fish faecal pellets, contain abundant preserved radiolarian tests (Fig. 5e and f). The concretions are interpreted to have precipitated exceptionally early, before any sediment compaction, because the contents are rafted and uncrushed (Emmings et al., 2020a). Rarity of radiolarian tests in the matrix surrounding radiolarian-bearing concretions (e.g., Fig. 5a and b) indicates widespread diagenetic mobilisation of biogenic (radiolarian) silica. This shows biogenic silica was a credible source for most or all quartz cements observed. An inherently high dissolved silica content in Palaeozoic seawater (Canfield et al., 2005; Conley et al., 2017; Siever, 1991) and/or elevated dissolved silica content supplied from local deltas or vents (Dunham and Wilson, 1985), potentially promoted colonisation

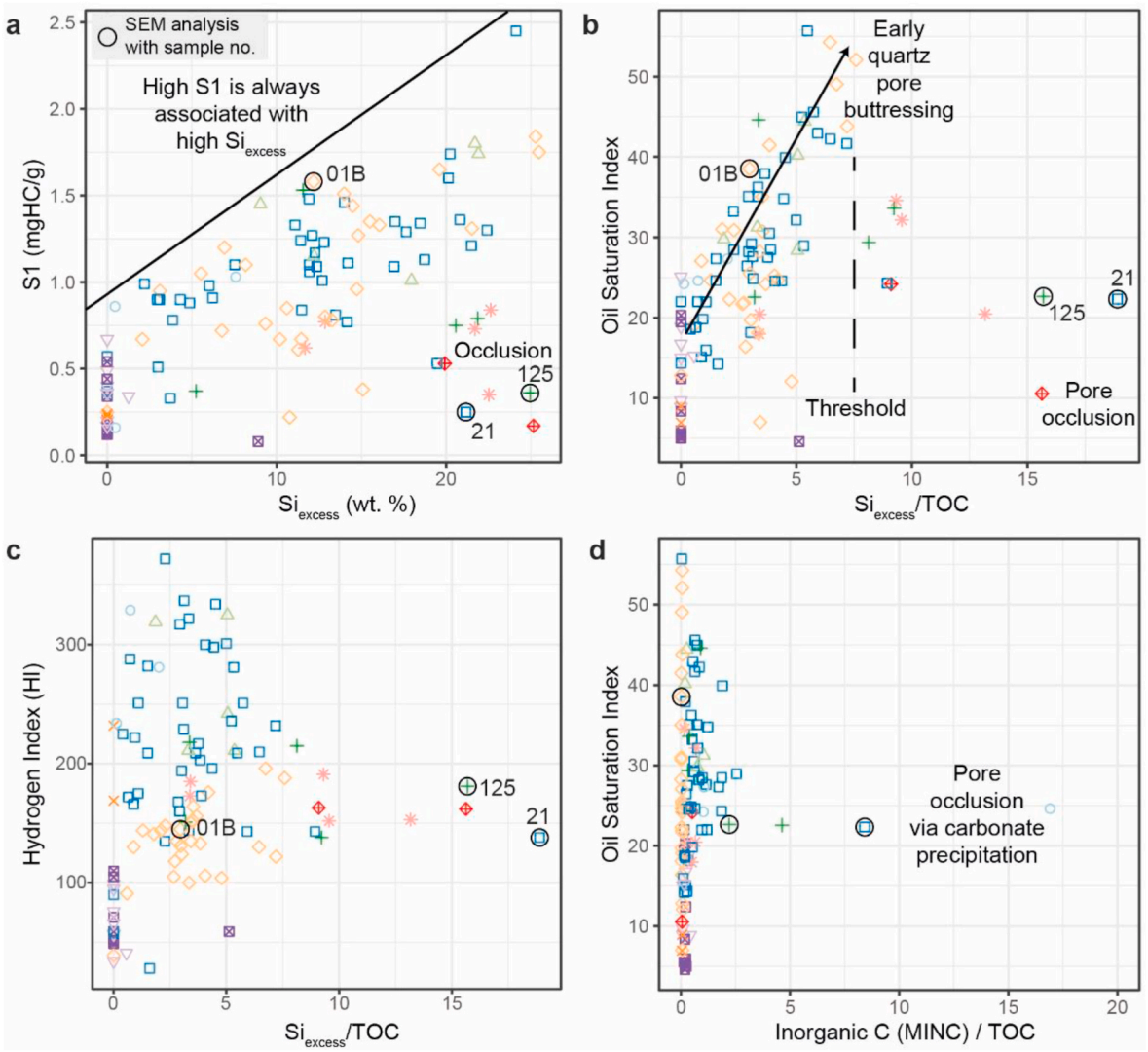

Fig. 7. Selected Rock-Eval pyrolysis parameters plotted versus Si_{excess} and carbonate content (MINC), and with interpretations annotated. (a) 'Free' hydrocarbon yield (S1) versus Si_{excess} shows high S1 and Si_{excess} content are weakly coupled. The exception of very low S1 and high Si_{excess} is best explained by pore occlusion by quartz and/or carbonate cements. (b) Oil saturation index (OSI) versus Si_{excess}/TOC shows positive correlation up to a threshold of ca. 7.5 Si_{excess}/TOC, suggesting precipitation of quartz cements buttressed (and prevented collapse of) pores and/or strengthened grains during early diagenesis. (c) HI and Si_{excess}/TOC are not correlated. (d) OSI versus MINC/TOC suggests significant pore occlusion via carbonate precipitation is minimal.

by radiolaria (assuming sufficient availability of other growth-limiting nutrients; see Conley et al., 2017 and references therein). Absence of quartz cement in Facies G-I is best explained by deposition under relatively low productivity, ventilated conditions (Emmings et al., 2020b); this process likely exerted a dual control on silica diagenesis via; (i) greatly reduced (or absence of) biogenic silica exported to seabed, and; (ii) diminished availability of catalysts for quartz fixation (e.g., Fe oxides).

Candidate substrates for anoxic marine weathering include volcanic glass or trioctahedral smectite (e.g., Mg-clays; Christidis and Koutsopoulou, 2013); the latter potentially derived from input of physical weathering products (detrital silicate grains), from volcanic input or generated via 'reverse weathering' during very early diagenesis (Michalopoulos and Aller, 2004; Michalopoulos et al., 2000), prior to anoxic marine weathering. One definition of reverse weathering is the reaction between biogenic opal, metal hydroxides, dissolved cations and HCO_3^- to produce cation-rich clays and CO_2 (Wallmann et al., 2008) (Eq. (3)); a precipitation reaction between continental chemical weathering products (Michalopoulos and Aller, 2004). K and Mg-bearing clays present as infill of encased (calcite-cemented) bioclasts, indicates operation of reverse weathering reactions, at least locally (Fig. 6). It is difficult to fully assess the role of reverse weathering, however, because the products of this reaction were potentially entirely consumed by subsequent marine weathering reactions.

$$\text{Biogenic opal} + \text{metal hydroxides} + \text{dissolved cations} + HCO_3^- \rightarrow \text{cation-rich silicates} + CO_2 \quad (3)$$

In summary, most or all (and at least some) quartz cements likely precipitated directly from biogenic silica opal A (Eq. (1)), perhaps with a short-lived opal CT intermediary, prior or concomitantly with reverse weathering. In addition, some or most of the authigenic quartz *possibly* also precipitated via marine silicate weathering of reactive cation-rich phases (Eq. (2)), including dissolution of reverse weathering products (Eq. (3)). The stoichiometry of silicate weathering suggests the ratio of dissolved silica versus clay minerals derived from this reaction is likely to be very low (Wallmann et al., 2008). At least ca. 50% quartz by volume (e.g., Fig. 5a) therefore suggests opal A/CT recrystallization was quantitatively more important, in terms of quartz precipitation, rather than silicate weathering. Since reverse weathering requires a source of dissolved silica, both mechanisms implicate biogenic opal as a key

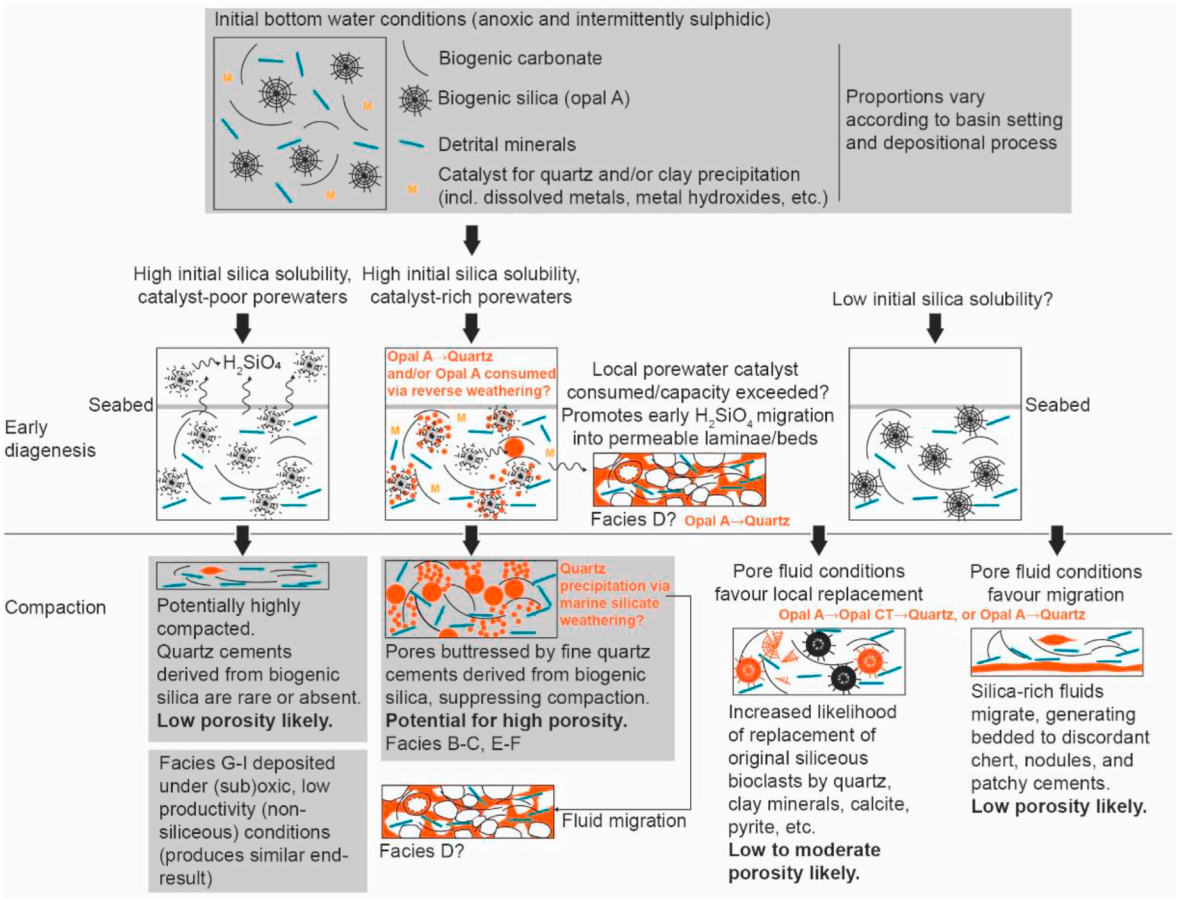

Fig. 8. Model for the early diagenetic quartz pore buttress effect in the Bowland Shale Formation. Quartz likely precipitated rapidly in Facies B-C and E-F (i.e., during early diagenesis); it is unclear whether this reaction proceeded via a short-lived opal CT intermediate phase.

precursor phase.

4.1. *Implications: evidence for pore buttressing by authigenic quartz*

Early diagenetic quartz cementation exerts a key control on mudstone compaction and thus porosity, permeability and potential for overpressure (e.g., Wangen, 2000; White et al., 2011). Petrographic observations (e.g., Fig. 4a–f; 5a-b) show quartz crystals form a 'buttressing' framework within the matrix of the Facies B-C and E-F. Using RockEval pyrolysis S1 (free hydrocarbons) and oil saturation index (OSI; see Materials and Methods) as proxies for oil-charged pores, we propose early diagenetic precipitation of quartz crystals suppressed pore collapse and therefore improved fluid storage capacity in Facies B-C and E-F. Correlation between Si_{excess} versus S1 (Fig. 7a), and Si_{excess} versus OSI (Fig. 7b), is best explained by oil-charging of pores buttressed by quartz. Lack of correlation between Si_{excess}/TOC and HI (Fig. 7c) shows coupled input of biogenic silica and oil-prone organic matter is not a credible explanation for the positive relationship between OSI and Si_{excess} (Fig. 7b).

Early diagenetic quartz precipitation likely initially partially filled open pores (therefore initially lowering porosity); the resultant buttressing network of quartz crystals, however, ensured the remaining pores were much more resistant to closure. Thus samples with high Si_{excess} also exhibit high OSI because an increased density of quartz crystals reduced compressibility during burial, enhancing preservation of pore space. This is in contrast to clay-rich, highly compressible (low Si_{excess}) samples. Quartz buttressing promoted preservation of intergranular porosity and likely limited the re-alignment of detrital or early diagenetic clay flocs (i.e., end on end or edge-edge aligned) during physical compaction (Velde, 1996). In addition, this process suppressed collapse of amorphous organic particles, as supported by petrographic observations (see Emmings et al., 2020a), preserving intragranular pores within organic matter.

Samples with Si_{excess}/TOC >7.5 progressively exhibit reduced OSI (Fig. 7b; typically Facies D and associated Facies E beds; and rarely B); this is interpreted as a result of pore occlusion by relatively 'late' quartz cement and/or carbonate cement. Pervasive cementation in Facies D is consistent with microscopic observations (sample 125; Fig. 4a–c, g-i). This is interpreted as a paragenetically late diagenetic phase of pore occlusion, prior to oil generation, which operated along porous and permeable laminae (Fig. 4g–i). Carbonate content exerts an autodilution effect on TOC (Fig. 2), but substantial pore occlusion is limited to Facies B where it directly overlies Facies A (Fig. 7d). Moderate to low OSI in sample 21 (Facies B overlying Facies A) is best explained by the combination of pervasive, dispersed quartz *and* carbonate cement within the matrix (Fig. 4a–c, 5a-b; 6).

A spectrum of quartz cementation styles in mudstones is envisaged (Fig. 8). In the Bowland Shale, early diagenetic quartz precipitation was apparently triggered by high initial opal A solubility and porewater conditions favourable for rapid nucleation of opal CT followed by quartz, or directly from opal A to quartz. Either process was likely facilitated by lowering of opal CT porewater saturation, perhaps via localised high porewater alkalinity, the presence of Fe oxides, or retardation by clay minerals or organic matter. A similar buttressing mechanism was proposed by Fishman et al. (2015) for cementation in the upper shale member of the Bakken Formation ('Facies Association 1'). In

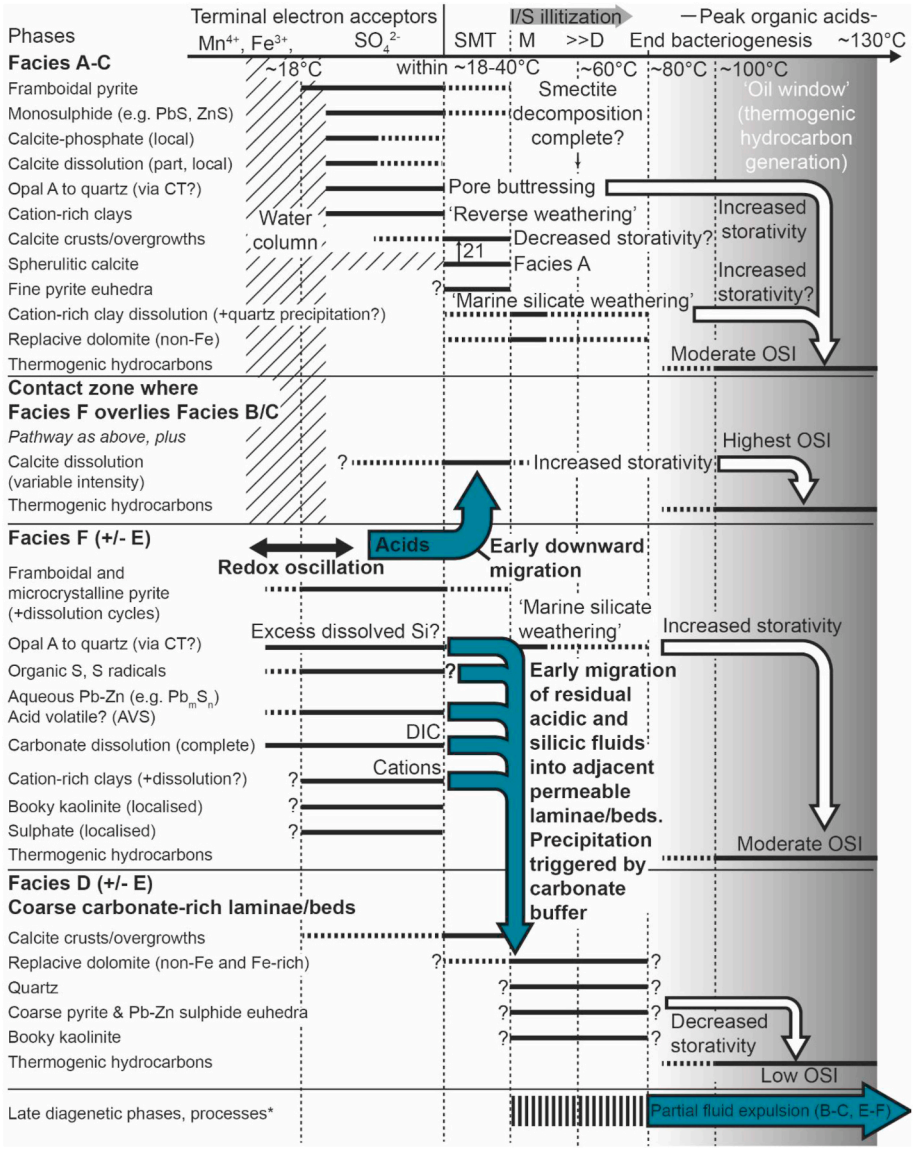

Fig. 9. Interpreted syngenetic and early diagenetic paragenetic sequence for anoxic facies (A–F), based on integration of observations and interpretations by Emmings (2018), Emmings et al. (2019), Emmings et al. (2020a, 2020b) and this study. Each row (phase) represents a formation/precipitation reaction unless otherwise stated. Diagenetic zones are based on Curtis (1977). Temperature ranges for diagenetic zones are equivocal. The depth of SMT likely fluctuated through time (within ca. 18 °C and 40 °C). An SMT intermittently close to 18 °C is considered likely if based on observations of sediment cores from the West African upwelling zone, an area defined by organic-rich sediments and high sediment accumulation rates (see Wefer et al., 1998; Moore et al., 2004). An SMT between 18 and 40 °C is supported by carbonate isotope data from Facies A (see Emmings et al., 2020b). Smectite decomposition temperature from Boles and Franks (1979). Oil window temperature range based on Jarvie and Lundell (2001). A bottom water temperature of 18 °C is based on the Cariaco Basin (Alvera-Azcárate et al., 2011) assuming this is a partial modern analogue for Craven Basin (Emmings et al., 2020b). End bacteriogenesis and peak organic acid temperature range from Yuan et al. (2019). *Late diagenetic phases in the Bowland Shale include calcite-cemented fractures (e.g., Clarke et al., 2018). SMT = sulphate reduction-methanogenesis transition zone. M = zone of methanogenesis. ≫D = zone dominated by decarboxylation reactions. AVS = acid-volatile (Pb, Zn) sulphide (e.g., Cooper and Morse, 1998; Landner and Reuther, 2005); DIC = dissolved inorganic C. OSI = Oil Saturation Index. Note Facies A exhibits very low storage capacity due to pervasive precipitation of spherulitic calcite associated with shallow anaerobic oxidation of methane. Where Facies B directly overlies Facies A (arrow labelled '21', e.g., sample 21), low fluid storage capacity is best explained by enhanced calcite mantling and precipitation within the matrix (Figs. 2 and 6).

comparison to siliceous mudstones in the Cline Shale, as described by Peng et al. (2020), Facies B-F best compare to Type B and/or Type C siliceous mudstones, whereas Facies G-I best compare to Type A argillaceous mudstones.

4.2. Paragenetic sequences

Simplified paragenetic sequences for anoxic facies (A-F) (Fig. 9) synthesise recent observations and interpretations with respect to the Bowland Shale (Emmings, 2018; Emmings et al., 2019, 2020a, 2020b). Facies B-C and F most closely resemble 'hemipelagic muds' (i.e., not deposited en-masse), which were deposited under contrasting (and cycling) Eh conditions, and are interbedded with Facies D and E (mass transport deposits). Emmings et al. (2020b) showed early diagenetic redoxclines migrated through the shallow sediment column relatively quickly during deposition of Facies A-F. The upper boundary of the sulphate-methane transition zone was likely positioned within decimetres (i.e., 10 s cm) to metres below seabed (Emmings et al., 2020b). Lack of evidence for overprint of the redox-sensitive metal record (primarily associated with sulphides and organic matter; Emmings et al., 2020b) suggests closed system conditions developed in Facies B-C and F during early diagenesis. The following section details a series of simplified paragenetic relationships for all anoxic facies (A-F).

Facies B-C mudstones are interpreted to represent deposition under the most strongly reducing conditions (i.e., relatively negative Eh) during periods of high sea level; anoxic and at least intermittently sulphidic bottom water conditions (Fig. 9). This is consistent with a variety of textural and geochemical proxy evidences (see Emmings et al., 2020b), including abundant framboidal pyrite and early diagenetic monosulphide (e.g., ZnS; see Emmings, 2018). Exceptionally early phosphate precipitation coupled to quartz precipitation in Facies B is consistent with the evidence of locally acidic porewaters (i.e., partial dissolution of skeletal carbonate; Fig. 5d), conditions which promote phosphate fixation (Taylor and Macquaker, 2011). It is clear that one or more factors, perhaps localised high porewater alkalinity or the presence of Fe oxides (e.g., Kastner et al., 1977; Meister et al., 2014), sufficiently reduced porewater saturation in opal A and opal CT, enabling direct low temperature quartz precipitation. Indeed evidence for partial dissolution of primary (allochemical) carbonate during quartz precipitation suggests porewaters locally exhibited high alkalinity. Whilst the role of porewater composition is unresolved, the evidence shows early diagenetic quartz precipitation enhanced fluid storage capacity in Facies B-C (Figs. 4–9).

Calcite crusts in Facies B, often 'mantling' bioclasts, post-date reverse

weathering (Fig. 6) and indicate increased porewater pH, alkalinity and Ca saturation as requirements for calcite precipitation. Observations (and modelling) of modern diagenetic systems suggests calcite precipitation typically proceeds within the sulphate-methane transition zone via anaerobic oxidation of methane (e.g., Meister, 2013; e.g., methane-derived authigenic carbonate; e.g., Joseph et al., 2013). Precipitation of Facies A spherulitic limestones within the zone of anaerobic oxidation of methane, likely relatively close to seabed, is supported by textural observations and isotopic data (Emmings et al., 2020b). Sample 21 represents a thin (cm-scale) transitional zone where Facies A is directly overlain by Facies B (Fig. 2). Continued, localised shallow anaerobic oxidation of methane within this zone best explains combination of quartz crystals, abundant primary carbonate *and* discrete calcite crystals and mantled calcite (Fig. 6). Dual quartz and carbonate cementation within the matrix reduced fluid storage capacity in sample 21 (Fig. 9). The majority of Facies B-C samples, however, do not exhibit such discrete carbonate cements (thus retaining high fluid storage capacity due to quartz buttressing). This is likely related to an expanded and deepened base of the sulphate-methane transition zone (Emmings et al., 2020b), considered less favourable for calcite precipitation within the matrix. CO_2 generated during methanogenesis was likely at least partially consumed via precipitation of dolomite coupled to marine silicate weathering (e.g., Torres et al., 2020, Fig. 9). This is supported by observations of relatively late diagenetic replacement of primary and mantled calcite with non-ferroan dolomite in Facies B (Figs. 5d and 6).

Falling sea level likely increased the export of reactive Fe from the shelf into the basin, prompting 'redox oscillation' between zones of Fe and sulphate reduction (i.e., generally less negative Eh), during deposition of Facies F muds. Oscillation between ferruginous and sulphidic bottom water states significantly complicate the early diagenetic paragenetic sequence for Facies F (Fig. 9), including; multiple phases of pyrite and sulphate precipitation associated with anaerobic oxidation of pyrite; long-lived organic matter degradation, and; complete carbonate dissolution under acidic conditions (Emmings et al., 2020b). Despite this, quartz precipitation was apparently robust to, and unaffected by, changing porewater Eh and pH (i.e., quartz textures are broadly similar in both Facies B and F). DeMaster (2003) suggested the dynamic range for pH during early diagenesis is potentially sufficiently small so that variations in pH produce minimal change in terms of silica solubility. Thus Facies F exhibits relatively high fluid storage capacity. Downward advection or diffusion of acidic fluids following quartz precipitation apparently enhanced porosity (therefore storage capacity), by triggering dissolution of phases such as carbonate and/or reactive silicates dispersed between the quartz crystals. This mechanism potentially explains why the highest OSI occurs at the contacts between Facies B/C and overlying Facies F mudstones (Fig. 2).

Absence of discrete ZnS in Facies F suggests Zn, likely together with Pb (both with faster H_2O exchange kinetics than Fe; Morse and Luther, 1999), was initially retained in solution under weakly reducing and acidic conditions (e.g., Cooper and Morse, 1998). Precipitation as solid sulphides (e.g., ZnS, PbS) via reaction with H_2S was potentially blocked due to complexation with polysulphides (or another presently unresolved complex; e.g., Rickard, 2012a), considered stable under relatively low Eh conditions (Rickard, 2012b). Such aqueous Zn and Pb species potentially (at least initially) complexed with organic matter (e.g., Holman et al., 2014), as supported by relatively high organic S (S_{org}) content (Emmings et al., 2019). Subsequently or alternatively, Zn and Pb aqueous species migrated within acidic fluids, enriched in dissolved inorganic C and other cations, from Facies F into Facies D laminae and beds during 'relatively' late diagenesis (Fig. 9). Such fluids are the proposed source for the interlocking quartz-calcite-dolomite-kaolinite-monosulphide cements in Facies D, which significantly decreased porosity and permeability, therefore fluid storage capacity (Fig. 4g).

The exact timing of cementation in Facies D is uncertain. Calcite mantling pre-dates the interlocking cements (Emmings, 2018), suggesting precipitation likely proceeded within the sulphate-methane transition zone, or within the zone of methanogenesis or decarboxylation (Fig. 9). Dissolved silica was potentially generated early (Fig. 8), particularly if local porewater catalysts for opal CT/quartz precipitation were exhausted/saturated. Alternatively, Facies D quartz and kaolinite cementation proceeded during 'late' early diagenesis (prior to oil generation), using migrated silica generated from marine silicate weathering or possibly related to silica phase transitions (e.g., illitization; Fig. 8). Cementation in Facies D coeval with illitization (i.e., dissolution and re-precipitation, collapse) of clays pinned between quartz grains in the matrix of surrounding Facies F muds is a particularly attractive mechanism because the process potentially generated overpressure (thus promoting fluid migration).

4.3. Synthesis

In summary, anoxic facies in the Bowland Shale contain abundant biogenic Si, now manifested as pervasive early diagenetic dispersed quartz cements. This is important for several reasons. Firstly, it enhances brittleness (e.g., Slatt, 2011; Rybacki et al., 2016; Peng et al., 2020) and in most cases fluid storage capacity (Fig. 7), and is therefore important for understanding the Bowland Shale as a target for unconventional oil or gas. This is particularly relevant in shale oil and shale gas systems, where oil retained in pores cracks to gas, rather than where gas is generated directly from kerogen (e.g., Jarvie et al., 2007). In contrast, sediments deposited under suboxic to oxic conditions (Facies G-I), proximal to the Pendle delta system, lack pervasive cement (e.g., Emmings et al., 2020a, b). Secondly, standard compaction curves (e.g., Velde, 1996) may be impacted by the quartz buttress effect, which could lead to spurious estimations or interpretations of mean sediment accumulation rates (when corrected for timespan; e.g., log-log 'Sadler' biplots; Sadler, 1981, 1999; Emmings et al., 2020a).

Increased storage capacity linked to early diagenetic quartz buttressing is also important with respect to mineral systems. The Bowland Shale apparently exhibited a high capacity for retention of fluids, originally derived from anoxic (ferruginous to euxinic) bottom waters, during diagenesis. This is important particularly in mineral deposits generated via mixing of several fluids, such as Pb-Zn systems, which are linked to supply of reduced S and/or metals during deposition or dewatering of organic-rich muds including the Bowland Shale (Kendrick et al., 2002; related to e.g., Navan-type; e.g., Ashton et al., 2016, and Pennine-type deposits; Dunham and Wilson, 1985).

Thus the Bowland Shale possibly defines a black shale sub-class with the following attributes; (i) the ability to host (and potentially transfer) a relatively large volume of early diagenetic fluids, derived from anoxic (ferruginous to euxinic) seawater, likely ligand- and/or metal-bearing (this study; Facies B-C, E-F); (ii) a sustained and high mean sediment accumulation rate (Emmings et al., 2020a) coupled to a high probability of encasement by highly cemented (thus likely low permeability) beds (e.g., Facies D), which promoted overpressure development (Frazer et al., 2014); (iii) a low early diagenetic compressibility (i.e., via early quartz buttressing, this study) but with a high likelihood of increasing compressibility during late diagenesis via temperature-driven clay mineral transformation reactions (e.g., illitization, Boles and Franks, 1979, particularly of clays pinned between quartz crystals); (iv) heterogeneous fill (i.e., interbedded carbonate-clastic facies; Emmings et al., 2020a) with high effective anisotropy, promoting lateral fluid flow (i.e., along Facies D beds), and; (v) positioned adjacent to carbonate-cemented (thus high-rigidity) platforms. Such properties, as originally proposed by Frazer et al. (2014), are considered favourable for Pb-Zn mineralisation.

Finally, quartz cementation is localised (bed-scale, closed-system) and linked to a biogenic source (radiolarian tests) associated with relatively productive water column conditions overlying anoxic bottom waters (Emmings et al., 2019, 2020b). Presence of chert on the southern edge of the Askrigg block (Fig. 1b) (Fairbairn, 2001) suggests these conditions were relatively widespread. Textural evidence (Fig. 6) also

shows operation of reverse weathering during early diagenesis, consistent with observations in partially analogous modern diagenetic systems (Michalopoulos and Aller, 2004; Michalopoulos et al., 2000; Wallmann et al., 2008). This indicates the Bowland Shale was potentially an important sink for seawater cations (e.g., K, Mg, Li, F; see Michalopoulos and Aller, 2004; Wallmann et al., 2008). More broadly, Mississippian anoxic, organic and mud-rich successions were clearly subject to highly dynamic early diagenetic processes, with implications for related hydrocarbon and mineral systems.

5. Conclusions

Integrated microscopic and bulk geochemical observations show siliceous mudstones in the Bowland Shale contain 'excess silica' and are quartz-cemented. Key conclusions are:

1. The distribution of quartz cementation is linked to the input of abundant, highly labile radiolarian tests under productivity-driven water column conditions;
2. Dissolution of the siliceous tests during early diagenesis is interpreted as the key source of silica required for quartz precipitation. At least ca. 50% silica cement by volume suggests precipitation within 10s–100 s m of seabed and implicates a biogenic source;
3. Dissolved silica was also partially consumed (at least initially) via the precipitation of authigenic clay minerals ('reverse weathering'), suggesting the Bowland Shale was an important sink for key cations dissolved in seawater;
4. Positive correlation between oil saturation index and excess silica, supplemented with microscopic observations, indicates early diagenetic quartz precipitation suppressed pore collapse, and therefore retained the pore space capacity, in order to host oil;
5. Pore buttressing during early diagenesis is a key aspect of understanding coupled brittleness and fluid storage capacity in the Bowland Shale. Therefore metre-scale siliceous packages in the Bowland Shale likely represent more prospective units within the Bowland Shale;
6. Evidence for multiple-phases of quartz and clay mineral precipitation and relatively low oil saturation content in relatively coarse, silt-rich facies suggests a paragenetically late diagenetic phase of pore occlusion operated along permeable laminae. Encasement by highly cemented (thus likely low permeability) beds potentially promoted overpressure development;
7. Early diagenetic quartz pore buttressing suggests the Bowland Shale exhibited a high capacity for retention of fluids originally derived from ferruginous anoxic to euxinic bottom waters. Thus the Bowland Shale possibly defines a black shale sub-class with the ability to host (and possibly transfer) a relatively large volume of early diagenetic fluids, which were potentially S- and/or metal-bearing. This is particularly relevant to understanding the genesis of adjacent (Pennine-type) Pb-Zn deposits, which were likely generated from fluids enriched in ligands (e.g., reduced S) and/or metals expelled from the Bowland Shale during diagenesis.

Declaration of competing interest

The authors declare that they have no known competing financial interests or personal relationships that could have appeared to influence the work reported in this paper.

CRediT authorship contribution statement

Joseph F. Emmings: Conceptualization, Methodology, Formal analysis, Investigation, Writing - original draft, Writing - review & editing, Visualization, Data curation, Project administration. **Patrick J. Dowey:** Conceptualization, Methodology, Formal analysis, Investigation, Writing - original draft, Writing - review & editing, Visualization. **Kevin G. Taylor:** Supervision, Funding acquisition, Writing - review & editing, Resources. **Sarah J. Davies:** Supervision, Writing - review & editing. **Christopher H. Vane:** Funding acquisition, Resources, Writing - review & editing. **Vicky Moss-Hayes:** Investigation, Resources. **Jeremy C. Rushton:** Writing - original draft, Writing - review & editing.

Acknowledgements

This research was part-funded by the British Geological Survey and contains PhD outputs (JE) funded by the Natural Environment Research Council (NERC) [grant no. NE/L002493/1] within the Central England Training Alliance (CENTA). We acknowledge the support of the University of Leicester XRF laboratory (Lin Marvin, Tom Knott). We acknowledge the support of the NERC-funded Nanoscale Imaging and Analysis Facility for Environmental Materials (NIAFEM) Facility in the Williamson Research Centre for Molecular Environmental Science, University of Manchester (NERC CC042), and the assistance of Jonathan Fellowes. We thank Kitty Milliken and several anonymous reviewers for their detailed and constructive reviews. Published with permission of the Director of the British Geological Survey.

Appendix A. Supplementary data

Supplementary data to this article can be found online at https://doi.org/10.1016/j.marpetgeo.2020.104567.

References

Alvera-Azcárate, A., et al., 2011. Thermocline characterisation in the Cariaco basin: a modelling study of the thermocline annual variation and its relation with winds and chlorophyll-a concentration. Continent. Shelf Res. 31 (1), 73–84. https://doi.org/10.1016/j.csr.2010.11.006.

Anderson, I., Underhill, J.R., 2020. Structural constraints on lower Carboniferous shale gas exploration in the Craven Basin, NW England. Petrol. Geosci. 26 (2), 303–324. https://doi.org/10.1144/petgeo2019-125.

Andrews, I.J., 2013. The Carboniferous Bowland Shale Gas Study: Geology and Resource Estimation. British Geological Survey for Department of Energy and Climate Change.

Arthurton, R.S., 1984. The Ribblesdale fold belt, NW England—a Dinantian-early Namurian dextral shear zone. Geol. Soc. Lond. Spec. Publ. 14 (1), 131–138. https://doi.org/10.1144/gsl.sp.1984.014.01.13.

Ashton, J.H., et al., 2016. The Giant Navan carbonate-hosted Zn–Pb deposit: exploration and geology: 1970–2015. B. Appl. Earth Sci. 125 (2), 75–76. https://doi.org/10.1080/03717453.2016.1166607.

Behl, R.J., 2011. Chert spheroids of the Monterey Formation, California (USA): early-diagenetic structures of bedded siliceous deposits. Sedimentology 58 (2), 325–351. https://doi.org/10.1111/j.1365-3091.2010.01165.x.

Behl, R.J., Garrison, R., 1994. The Origin of Chert in the Monterey Formation of California (USA). Siliceous, Phosphatic and Glauconitic Sediments of the Tertiary and Mesozoic. Proc. 29. International Geological Congress, Part C. VSP, Utrecht, pp. 101–132.

Bijkerk, J.F., 2014. External Controls on Sedimentary Sequences: a Field and Analogue Modelling-Based Study.

Bjørlykke, K., 2011. Open-system chemical behaviour of Wilcox Group mudstones. How is large scale mass transfer at great burial depth in sedimentary basins possible? A discussion. Mar. Petrol. Geol. 28 (7), 1381–1382. https://doi.org/10.1016/j.marpetgeo.2011.01.009.

Boles, J.R., Franks, S.G., 1979. Clay diagenesis in Wilcox sandstones of Southwest Texas; implications of smectite diagenesis on sandstone cementation. J. Sediment. Res. 49 (1), 55–70. https://doi.org/10.1306/212f76bc-2b24-11d7-8648000102c1865d.

Bouch, J.E., et al., 2006. Direct evidence of fluid mixing in the formation of stratabound Pb–Zn–Ba–F mineralisation in the Alston block, north Pennine orefield (England). Miner. Deposita 41 (8), 821–835. https://doi.org/10.1007/s00126-006-0093-3.

Boucot, A., et al., 2013. Phanerozoic Paleoclimate: an Atlas of Lithologic Indicators of Climate. Concepts in Sedimentology and Palaeontology No. 11. Society for Sedimentary Geology, Tulsa, Oklahoma, USA.

Brandon, A, et al., 1998. Geology of the Country Around Lancaster: memoir for 1:50 000 sheet 5. The Stationary Office, London.

Browne, M.A.E., et al., 1999. A Lithostratigraphical Framework for the Carboniferous Rocks of the Midland Valley of Scotland. British Geological Survey Research Report. RR/99/07.

Canfield, D.E., et al., 2005. The silicon cycle. In: Canfield, D.E., Kristensen, E., Thamdrup, B. (Eds.), Advances in Marine Biology. Academic Press, pp. 441–463. https://doi.org/10.1016/S0065-2881(05)48012-8.

Casey, R., 1993. Radiolaria. In: Lipps, J. (Ed.), Fossil Prokaryotes and Protists, Boston, Massachusetts, pp. 249–284.

Christidis, G.E., Koutsopoulou, E., 2013. A simple approach to the identification of trioctahedral smectites by X-ray diffraction. Clay Miner. 48 (5), 687–696. https://doi.org/10.1180/claymin.2013.048.5.22.
Clarke, H., et al., 2018. Shale gas resources of the Bowland Basin, NW England: a holistic study. Petrol. Geosci. 24 (3), 287–322. https://doi.org/10.1144/petgeo2017-066.
Collinson, J.D., 1988. Controls on Namurian sedimentation in the central province basins of northern England. In: Besly, B.M., Kelling, G. (Eds.), Sedimentation in a Synorogenic Basin Complex: the Upper Carboniferous of Northwest Europe. Blackie, Glasgow, pp. 85–101.
Conley, D.J., et al., 2017. Biosilicification drives a decline of dissolved Si in the oceans through geologic time. Front. Mar. Sci. 4 (397) https://doi.org/10.3389/fmars.2017.00397.
Cooper, D.C., Morse, J.W., 1998. Extractability of metal sulfide minerals in acidic Solutions: application to environmental studies of trace metal contamination within anoxic sediments. Environ. Sci. Technol. 32 (8), 1076–1078. https://doi.org/10.1021/es970415t.
Curtis, C.D., 1977. Geochemistry: sedimentary geochemistry: environments and processes dominated by involvement of an aqueous phase. Phil. Trans. Roy. Soc. Lond. Math. Phys. Sci. 286 (1336), 353–372. https://doi.org/10.1098/rsta.1977.0123.
Davies, S.J., 2008. The record of Carboniferous sea-level change in low-latitude sedimentary successions from Britain and Ireland during the onset of the late Paleozoic ice age. Geol. Soc. Am. Spec. Pap. 441, 187–204. https://doi.org/10.1130/2008.2441(13.
Davies, S.J., et al., 2012. Sedimentary process control on carbon isotope composition of sedimentary organic matter in an ancient shallow-water shelf succession. G-cubed 13 (11), 1–15. https://doi.org/10.1029/2012GC004218.
DeMaster, D.J., 2003. 7.04 - the diagenesis of biogenic silica: chemical transformations occurring in the water column, seabed, and crust. In: Holland, H.D., Turekian, K.K. (Eds.), Treatise on Geochemistry. Pergamon, Oxford, pp. 87–98. https://doi.org/10.1016/B0-08-043751-6/07095-X.
Dixit, S., et al., 2001. Processes controlling solubility of biogenic silica and pore water build-up of silicic acid in marine sediments. Mar. Chem. 73 (3), 333–352. https://doi.org/10.1016/S0304-4203(00)00118-3.
Dowey, P.J., Taylor, K.G., 2017. Extensive authigenic quartz overgrowths in the gas-bearing Haynesville-Bossier Shale, USA. Sediment. Geol. 356, 15–25. https://doi.org/10.1016/j.sedgeo.2017.05.001.
Dowey, P.J., Taylor, K.G., 2019. Diagenetic mineral development within the upper Jurassic Haynesville-Bossier shale, USA. Sedimentology. https://doi.org/10.1111/sed.12624.
Drewery, S., et al., 1987. Provenance of Carboniferous sandstones from U-Pb dating of detrital zircons. Nature 325 (6099), 50–53.
Dunham, A.C., Wilson, A.A., 1985. Geology of the northern Pennine orefield: volume 2, stainmore to craven. Economic Memoir of the British Geological Survey.
Emmings, J., 2018. Controls on UK Lower Namurian Shale Gas Prospectivity: Understanding the Spatial and Temporal Distribution of Organic Matter in Siliciclastic Mudstones. PhD Thesis. University of Leicester.
Emmings, J., et al., 2017. Stream and slope weathering effects on organic-rich mudstone geochemistry and implications for hydrocarbon source rock assessment: a Bowland shale case study. Chem. Geol. 471, 74–91. https://doi.org/10.1016/j.chemgeo.2017.09.012.
Emmings, J.F., et al., 2020a. From marine bands to hybrid flows: sedimentology of a Mississippian black shale. Sedimentology 67 (1), 261–304. https://doi.org/10.1111/sed.12642.
Emmings, J.F., et al., 2019. Controls on amorphous organic matter type and sulphurization in a Mississippian black shale. Rev. Palaeobot. Palynol. 268, 1–18. https://doi.org/10.1016/j.revpalbo.2019.04.004.
Emmings, J.F., et al., 2020b. A Mississippian black shale record of redox oscillation in the Craven Basin, UK. Palaeogeogr. Palaeoclimatol. Palaeoecol. 538 https://doi.org/10.1016/j.palaeo.2019.109423.
Fairbairn, R.A., 2001. The stratigraphy of the Namurian great/main limestone on the Alston block, stainmore trough and Askrigg block of northern England. Proc. Yorkshire Geol. Polytech. Soc. 53 (4), 265–274. https://doi.org/10.1144/pygs.53.4.265.
Fishman, N.S., et al., 2015. Petrology and Diagenetic History of the Upper Shale Member of the Late Devonian–Early Mississippian Bakken Formation, Williston Basin, North Dakota, Paying Attention to Mudrocks: Priceless! Geological Society of America, 0.10.1130/2015.2515(07).
Fraser, A.J., Gawthorpe, R., 2003. An Atlas of Carboniferous Basin Evolution in Northern England. Geological Society, London. https://doi.org/10.1144/GSL.MEM.2003.028.01.08. Memoir 28.
Fraser, A.J., Gawthorpe, R.L., 1990. Tectono-stratigraphic development and hydrocarbon habitat of the Carboniferous in northern England, 55. Geological Society of London Special Publication, pp. 49–86. https://doi.org/10.1144/gsl.sp.1990.055.01.031.
Frazer, M., et al., 2014. Fluid expulsion from overpressured basins: implications for Pb–Zn mineralisation and dolomitisation of the East Midlands platform, northern England. Mar. Petrol. Geol. 55, 68–86. https://doi.org/10.1016/j.marpetgeo.2014.01.004.
Gawthorpe, R., 1987a. Tectono-sedimentary evolution of the Bowland basin, N England, during the Dinantian. J. Geol. Soc. 144, 59–71. https://doi.org/10.1144/gsjgs.144.1.0059.
Gawthorpe, R.L., 1987b. Burial dolomitization and porosity development in a mixed carbonate-clastic sequence: an example from the Bowland Basin, northern England. Sedimentology 34 (4), 533–558. https://doi.org/10.1111/j.1365-3091.1987.tb00785.x.
Grenne, T., Slack, J.F., 2003. Paleozoic and Mesozoic silica-rich seawater: evidence from hematitic chert (jasper) deposits. Geology 31 (4), 319–322. https://doi.org/10.1130/0091-7613(2003)031<0319:Pamsrs>2.0.Co;2.
Henry, D.G., et al., 2019. A rapid method for determining organic matter maturity using Raman spectroscopy: application to Carboniferous organic-rich mudstones and coals. Int. J. Coal Geol. 203, 87–98. https://doi.org/10.1016/j.coal.2019.01.003.
Henry, D.G., et al., 2018. Assessing low-maturity organic matter in shales using Raman spectroscopy: effects of sample preparation and operating procedure. Int. J. Coal Geol. 191, 135–151. https://doi.org/10.1016/j.coal.2018.03.005.
Hild, E., Brumsack, H.J., 1998. Major and minor element geochemistry of Lower Aptian sediments from the NW German Basin (core Hohenegglesen KB 40). Cretac. Res. 19 (5), 615–633. https://doi.org/10.1006/cres.1998.0122.
Hinman, N.W., 1990. Chemical factors influencing the rates and sequences of silica phase transitions: effects of organic constituents. Geochem. Cosmochim. Acta 54 (6), 1563–1574. https://doi.org/10.1016/0016-7037(90)90391-W.
Hinman, N.W., 1998. Sequences of silica phase transitions: effects of Na, Mg, K, Al, and Fe ions. Mar. Geol. 147 (1), 13–24. https://doi.org/10.1016/S0025-3227(98)00002-4.
Holdsworth, B., Collinson, J.D., 1988. Millstone Grit cyclicity revisited. In: Besly, B.M., Kelling, G. (Eds.), Sedimentation in a Synorogenic Basin Complex: the Upper Carboniferous of Northwest Europe. Blackie, Glasgow, pp. 132–152.
Holman, A.I., et al., 2014. New aspects of sulfur biogeochemistry during ore deposition from δ34S of elemental sulfur and organic sulfur from the Here's Your Chance Pb/Zn/Ag deposit. Chem. Geol. 387, 126–132. https://doi.org/10.1016/j.chemgeo.2014.08.025.
Hurd, D.C., 1973. Interactions of biogenic opal, sediment and seawater in the Central Equatorial Pacific. Geochem. Cosmochim. Acta 37 (10), 2257–2282. https://doi.org/10.1016/0016-7037(73)90103-8.
Iler, R.K., 1955. The colloid chemistry of silica and silicates. Soil Sci. 80 (1), 86.
Isaacs, C.M., 1982. Influence of rock composition on kinetics of silica phase changes in the Monterey Formation, Santa Barbara area. Calif. Geol. 10 (6), 304–308, 10.1130/0091-7613(1982)10<304:Iorcok>2.0.Co;2.
Jarvie, D.M., et al., 2007. Unconventional shale gas systems: the Mississippian Barnett Shale of north-central Texas as one model for thermogenic shale gas assessment. In: Hill, R.J., Jarvie, D.M. (Eds.), AAPG Bulletin Special Issue: Barnett Shale, pp. 475–499. https://doi.org/10.1306/12190606068.
Jarvie, D.M., Lundell, L.L., 2001. Chapter 15: amount, type and kinetics of thermal transformation of organic matter in the Miocene Monterey Formation. In: Isaacs, C., Rullkotter, J. (Eds.), The Monterey Formation: from Rocks to Molecules. Columbia University Press, New York, pp. 268–295.
Joseph, C., et al., 2013. Methane-derived authigenic carbonates from modern and paleoseeps on the Cascadia margin: mechanisms of formation and diagenetic signals. Palaeogeogr. Palaeoclimatol. Palaeoecol. 390, 52–67. https://doi.org/10.1016/j.palaeo.2013.01.012.
Kastner, M., et al., 1977. Diagenesis of siliceous oozes .1. Chemical controls on rate of opal-a to opal-CT transformation - experimental-study. Geochem. Cosmochim. Acta 41, 1041–1059. https://doi.org/10.1016/0016-7037(77)90099-0.
Keene, J.B., 1975. Cherts and porcellanites from the north Pacific. Initial Rep. Deep Sea Drill. Proj. 32, 429–507.
Kendrick, M.A., et al., 2002. Hydrothermal fluid origins in a fluorite-rich Mississippi valley-type district: combined noble gas (He, Ar, Kr) and halogen (Cl, Br, I) analysis of fluid inclusions from the south Pennine ore field, United Kingdom. Econ. Geol. 97 (3), 435–451. https://doi.org/10.2113/gsecongeo.97.3.435.
Kidder, D., Erwin, D., 2001. Secular distribution of biogenic silica through the Phanerozoic: comparison of silica-replaced fossils and bedded cherts at the series level. J. Geol. 109 (4), 509–522. https://doi.org/10.1086/320794.
Kominz, M.A., et al., 2011. Lithology dependence of porosity in slope and deep marine sediments. J. Sediment. Res. 81 (10), 730–742. https://doi.org/10.2110/jsr.2011.60.
Lancelot, Y., 1973. Chert and Silica Diagenesis in Sediments from the Central Pacific. Initial Reports of the Deep Sea Drilling Project, vol. 17. U.S. Government Printing Office, Washington.
Landner, L., Reuther, R., 2005. Speciation, Mobility and Bioavailability of Metals in the Environment, Metals in Society and in the Environment: A Critical Review of Current Knowledge on Fluxes, Speciation, Bioavailability and Risk for Adverse Effects of Copper, Chromium, Nickel and Zinc. Springer Netherlands, Dordrecht, pp. 139–274. https://doi.org/10.1007/1-4020-2742-7_6.
Lewis, C.L.E., et al., 1992. Elevated K/T palaeotemperatures throughout Northwest England: three kilometres of Tertiary erosion? Earth Planet Sci. Lett. 112 (1), 131–145. https://doi.org/10.1016/0012-821X(92)90012-K.
Mackenzie, F.T., Garrels, R.M., 1966. Chemical mass balance between rivers and oceans. Am. J. Sci. 264 (7), 507–525. https://doi.org/10.2475/ajs.264.7.507.
Meister, P., 2013. Two opposing effects of sulfate reduction on carbonate precipitation in normal marine, hypersaline, and alkaline environments. Geology 41 (4), 499–502. https://doi.org/10.1130/g34185.1.
Meister, P., et al., 2014. Early diagenetic quartz formation at a deep iron oxidation front in the Eastern Equatorial Pacific – a modern analogue for banded iron/chert formations? Geochem. Cosmochim. Acta 137, 188–207. https://doi.org/10.1016/j.gca.2014.03.035.
Merriman, R.J., Kemp, S.J., 1996. Clay minerals and sedimentary basin maturity. Mineral. Soc. Bull. 111 (7–8).
Michalopoulos, P., Aller, R.C., 1995. Rapid clay mineral Formation in Amazon delta sediments: reverse weathering and oceanic elemental cycles. Science 270 (5236), 614–617. https://doi.org/10.1126/science.270.5236.614.

Michalopoulos, P., Aller, R.C., 2004. Early diagenesis of biogenic silica in the Amazon delta: alteration, authigenic clay formation, and storage. Geochem. Cosmochim. Acta 68 (5), 1061–1085. https://doi.org/10.1016/j.gca.2003.07.018.
Michalopoulos, P., et al., 2000. Conversion of diatoms to clays during early diagenesis in tropical, continental shelf muds. Geology 28 (12), 1095–1098, 10.1130/0091-7613(2000)28<1095:CODTCD>2.0.CO;2.
Milliken, K.L., et al., 2016. Quartz types, authigenic and detrital, in the upper Cretaceous Eagle Ford formation, south Texas, USA. Sediment. Geol. 339, 273–288. https://doi.org/10.1016/j.sedgeo.2016.03.012.
Milliken, K.L., Olson, T., 2017. Silica Diagenesis, Porosity Evolution, and Mechanical Behavior In Siliceous Mudstones, Mowry Shale (Cretaceous), Rocky Mountains, U.S.A. J. Sediment. Res. 87 (4), 366–387. https://doi.org/10.2110/jsr.2017.24.
Moore Jr., T.C., 2008. Biogenic silica and chert in the Pacific Ocean. Geology 36 (12), 975–978. https://doi.org/10.1130/g25057a.1.
Moore, T.S., et al., 2004. Anaerobic methane oxidation and the formation of dolomite. Earth Planet Sci. Lett. 229 (1–2), 141–154. https://doi.org/10.1016/j.epsl.2004.10.015.
Morris, R.C., Fletcher, A.B., 1987. Increased solubility of quartz following ferrous–ferric iron reactions. Nature 330 (6148), 558–561. https://doi.org/10.1038/330558a0.
Morse, J.W., Luther, G.W., 1999. Chemical influences on trace metal-sulfide interactions in anoxic sediments. Geochem. Cosmochim. Acta 63 (19–20), 3373–3378. https://doi.org/10.1016/S0016-7037(99)00258-6.
Murata, K.J., Larson, R.R., 1975. Diagenesis of Miocene siliceous shales, Temblor Range, California. J. Res. U. S. Geol. Surv. 3 (5), 553–566.
Newport, S.M., et al., 2018. Sedimentology and microfacies of a mud-rich slope succession: in the Carboniferous Bowland Basin, NW England (UK). J. Geol. Soc. 175 (2), 247–262. https://doi.org/10.1144/jgs2017-036.
Parnell, J., et al., 2016. Selenium enrichment in Carboniferous Shales, Britain and Ireland: Problem or opportunity for shale gas extraction? Appl. Geochem. 66, 82–87. https://doi.org/10.1016/j.apgeochem.2015.12.008.
Pearson, M.J., Russell, M.A., 2000. Subsidence and erosion in the Pennine Carboniferous Basin, England: lithological and thermal constraints on maturity modelling. J. Geol. Soc. 157 (2), 471–482. https://doi.org/10.1144/jgs.157.2.471.
Peng, J., et al., 2020. Quartz types in the Upper Pennsylvanian organic-rich Cline Shale (Wolfcamp D), Midland Basin, Texas: Implications for silica diagenesis, porosity evolution and rock mechanical properties. Sedimentology 67 (4), 2040–2064. https://doi.org/10.1111/sed.12694.
Perry, E., Hower, J., 1972. Late-Stage Dehydration in Deeply Buried Pelitic Sediments. Am. Assoc. Petrol. Geol. Bull. 56 (10), 2013–2021.
Pharaoh, T., et al., 2019. The Môn-Deemster-Ribblesdale Fold-Thrust Belt, Central UK: a Concealed Variscan Inversion Belt Located on Weak Caledonian Crust. Geological Society, vol. 490. Special Publications, London, pp. SP490–2018, 109.10.1144/sp490-2018-109.
Ramsbottom, W.H.C., et al., 1962. Boreholes in the Carboniferous rocks of the Ashover district, Derbyshire. Bull. Geol. Surv. G. B. 19, 75–168.
Rice, S.B., et al., 1995. Application of Fourier transform infrared spectroscopy to silica diagenesis; the opal-A to opal-CT transformation. J. Sediment. Res. 65 (4a), 639–647. https://doi.org/10.1306/d4268185-2b26-11d7-8648000102c1865d.
Rickard, D., 2012a. Chapter 4 - Aqueous Metal–Sulfide Chemistry: Complexes, Clusters And Nanoparticles. In: Rickard, D. (Ed.), Developments in Sedimentology. Elsevier, pp. 121–194. https://doi.org/10.1016/B978-0-444-52989-3.00004-0.
Rickard, D., 2012b. Chapter 6 - Sedimentary Pyrite. In: David, R. (Ed.), Developments in Sedimentology. Elsevier, pp. 233–285. https://doi.org/10.1016/B978-0-444-52989-3.00006-4.
Rybacki, E., et al., 2016. What controls the mechanical properties of shale rocks? – Part II: Brittleness. J. Petrol. Sci. Eng. 144, 39–58. https://doi.org/10.1016/j.petrol.2016.02.022.
Sadler, P., 1999. The influence of hiatuses on sediment accumulation rates. GeoResearch Forum.
Sadler, P.M., 1981. Sediment Accumulation Rates and the Completeness of Stratigraphic Sections. J. Geol. 89 (5), 569–584.
Schieber, J., et al., 2000. Diagenetic origin of quartz silt in mudstones and implications for silica cycling. Nature 406 (6799), 981–985.
Schink, D.R., et al., 1975. Processes affecting the concentration of silica at the sediment-water interface of the Atlantic Ocean. J. Geophys. Res. 80 (21), 3013–3031. https://doi.org/10.1029/JC080i021p03013, 1896-1977.
Sholkovitz, E.R., Price, N.B., 1980. The major-element chemistry of suspended matter in the Amazon Estuary. Geochem. Cosmochim. Acta 44 (2), 163–171. https://doi.org/10.1016/0016-7037(80)90128-3.
Siever, R., 1991. Silica in the Oceans: Biological-Geochemical Interplay. MIT Press, Scientists on Gaia.
Slatt, R.M., 2011. Important geological properties of unconventional resource shales. Cent. Eur. J. Geosci. 3 (4), 435–448. https://doi.org/10.2478/s13533-011-0042-2.
Smith, N., et al., 2011. UK data and analysis for shale gas prospectivity. Geol. Soc. Lond. Petrol. Geol. Conf. Ser. 7 (1), 1087–1098. https://doi.org/10.1144/0071087.
Spears, D.A., 2006. Clay mineralogy of onshore UK Carboniferous mudrocks. Clay Miner. 41 (1), 395–416. https://doi.org/10.1180/0009855064110201.
Spears, D.A., et al., 1999. Namurian bentonites in the Pennine Basin, UK – origin and magmatic affinities. Sedimentology 46 (2), 385–401. https://doi.org/10.1046/j.1365-3091.1999.00220.x.
Stephenson, M.H., et al., 2008. Palaeoecological and possible evolutionary effects of early Namurian (Serpukhovian, Carboniferous) glacioeustatic cyclicity. J. Geol. Soc. 165 (6), 993–1005. https://doi.org/10.1144/0016-76492007-153.
Taylor, K.G., Macquaker, J.H.S., 2011. Iron Minerals in Marine Sediments Record Chemical Environments. Elements 7 (2), 113–118. https://doi.org/10.2113/gselements.7.2.113.
Taylor, K.G., Macquaker, J.H.S., 2014. Diagenetic alterations in a silt- and clay-rich mudstone succession: an example from the Upper Cretaceous Mancos Shale of Utah, USA. Clay Miner. 49 (2), 213–227. https://doi.org/10.1180/claymin.2014.049.2.05.
Thyberg, B., Jahren, J., 2011. Quartz cementation in mudstones: sheet-like quartz cement from clay mineral reactions during burial. Petrol. Geosci. 17 (1), 53–63. https://doi.org/10.1144/1354-079310-028.
Thyberg, B., et al., 2010. Quartz cementation in Late Cretaceous mudstones, northern North Sea: Changes in rock properties due to dissolution of smectite and precipitation of micro-quartz crystals. Mar. Petrol. Geol. 27 (8), 1752–1764. https://doi.org/10.1016/j.marpetgeo.2009.07.005.
Torres, M.E., et al., 2020. Silicate weathering in anoxic marine sediment as a requirement for authigenic carbonate burial. Earth Sci. Rev. 200, 102960. https://doi.org/10.1016/j.earscirev.2019.102960.
Tribovillard, N., et al., 2006. Trace metals as paleoredox and paleoproductivity proxies: An update. Chem. Geol. 232, 12–32. https://doi.org/10.1016/j.chemgeo.2006.02.012.
Van Beueskom, J.E.E., et al., 1997. Aluminium and silicic acid in water and sediments of the Enderby and Crozet Basins. Deep Sea Res. Part II Top. Stud. Oceanogr. 44 (5), 987–1003. https://doi.org/10.1016/S0967-0645(96)00105-1.
Velde, B., 1996. Compaction trends of clay-rich deep sea sediments. Mar. Geol. 133 (3), 193–201. https://doi.org/10.1016/0025-3227(96)00020-5.
Wallmann, K., et al., 2008. Silicate weathering in anoxic marine sediments. Geochem. Cosmochim. Acta 72 (12), 2895–2918. https://doi.org/10.1016/j.gca.2008.03.026.
Walters, S.G., Ineson, P.R., 1981. A review of the distribution of and the correlation of igneous rocks in Derbyshire, England. Mercian Geol. 8, 81–132.
Wang, J., et al., 2012. Petrology and geochemistry of chert on the marginal zone of Yangtze Platform, western Hunan, South China, during the Ediacaran–Cambrian transition. Sedimentology 59 (3), 809–829. https://doi.org/10.1111/j.1365-3091.2011.01280.x.
Wangen, M., 2000. Generation of overpressure by cementation of pore space in sedimentary rocks. Geophys. J. Int. 143 (3), 608–620. https://doi.org/10.1046/j.1365-246X.2000.00248.x.
Waters, C.N., et al., 2007. Lithostratigraphical Framework for Carboniferous Successions of Great Britain (Onshore). British Geological Survey Research Report. RR/07/01.
Waters, C.N., Condon, D.J., 2012. Nature and timing of Late Mississippian to Mid-Pennsylvanian glacio-eustatic sea-level changes of the Pennine Basin, UK. J. Geol. Soc. 169 (1), 37–51. https://doi.org/10.1144/0016-76492011-047.
Waters, C.N., et al., 2014. The Millstone Grit Group (Pennsylvanian) of the Northumberland–Solway Basin and Alston Block of northern England. Proc. Yorks. Geol. Soc. 60 (1), 29–51. https://doi.org/10.1144/pygs2014-341.
Waters, C.N., et al., 2019. Lithological and chemostratigraphic discrimination of facies within the Bowland Shale Formation within the Craven and Edale basins, UK. Petrol. Geosci. https://doi.org/10.1144/petgeo2018-039.
Waters, C.N., et al., 2009. A Lithostratigraphical Framework for the Carboniferous Successions of Southern Great Britain (Onshore). British Geological Survey Research Report. RR/09/01.
Wefer, G., et al., 1998. Site 1082. Proceedings of the Ocean Drilling Program; Initial Reports; Benguela Current; Covering Leg 175 of the Cruises of the Drilling Vessel JOIDES Resolution, Las Palmas, Canary Islands, to Cape Town, South Africa, Sites 1075-1087, 9 August-8 October, 1997, vol. 175, p. 273.
White, R.J., et al., 2011. Importance of volcanic glass alteration to sediment stabilization: offshore Japan. Sedimentology 58 (5), 1138–1154. https://doi.org/10.1111/j.1365-3091.2010.01198.x.
Whitelaw, P., et al., 2019. Shale gas reserve evaluation by laboratory pyrolysis and gas holding capacity consistent with field data. Nat. Commun. 10 (1), 3659. https://doi.org/10.1038/s41467-019-11653-4.
Wilkinson, J, 2014. Sediment-Hosted Zinc–Lead Mineralization. Treatise on Geochemistry. Elsevier, Oxford.
Williams, L.A., Crerar, D.A., 1985. Silica diagenesis; II, General mechanisms. J. Sediment. Res. 55 (3), 312–321. https://doi.org/10.1306/212f86b1-2b24-11d7-8648000102c1865d.
Wright, A.M., et al., 2010. Application of Inorganic Whole Rock Geochemistry to Shale Resource Plays. Canadian Unconventional Resources & International Petroleum Conference, pp. 19–21.
Yuan, G., et al., 2019. A review of feldspar alteration and its geological significance in sedimentary basins: From shallow aquifers to deep hydrocarbon reservoirs. Earth Sci. Rev. 191, 114–140. https://doi.org/10.1016/j.earscirev.2019.02.004.
Zijp, M., et al., 2017. Resource Estimation of Shale Gas and Shale Oil in Europe. Report T7b of the EUOGA Study (EU Unconventional Oil and Gas Assessment) Commissioned by European Commission Joint Research Centre to GEUS.